

MULTISCALE GRAIN-SIZE MAPPING ALONG THE UPPER SANDY RIVER

by

ERIC STEVEN LEVENSON

A THESIS

Presented to the Department of Geography
and the Division of Graduate Studies of the University of Oregon
in partial fulfillment of the requirements
for the degree of
Master of Science

June 2021

THESIS APPROVAL PAGE

Student: Eric Steven Levenson

Title: Multiscale Grain-Size Mapping Along the Upper Sandy River

This thesis has been accepted and approved in partial fulfillment of the requirements for the Master of Science degree in the Geography by:

Mark Fonstad	Chairperson
Patricia McDowell	Member

and

Andrew Karduna	Interim Vice Provost for Graduate Studies
----------------	---

Original approval signatures are on file with the University of Oregon Division of Graduate Studies.

Degree awarded June 2021

© 2021 Eric Steven Levenson



This work is licensed under a Creative Commons
Attribution-NonCommercial (United States) License.

THESIS ABSTRACT

Eric Steven Levenson

Master of Science

Department of Geography

June 2021

Title: Multiscale Grain-Size Mapping Along the Upper Sandy River

Grain-size remote sensing presents an opportunity to address our poor understanding of the relationships among the patterns and processes of sediment sorting across spatial scales and advance the accessibility to riverscape mapping approaches. This thesis confronts the barriers to applying image-based grain-size mapping techniques by presenting a methodological framework that addresses the principal components of photosieving and their implications for the resulting grain-size dataset. This framework is leveraged to develop a protocol for mapping the spatial variability in coarse sediment within gravel bars and throughout a 12 km segment of the upper Sandy River, Oregon, USA. I analyze the grain-size variability at the river segment and bar scales in relation to active channel width. The results illustrate that bar scale variability in some cases is nearly equivalent to the grain-size variability observed within the 12 km reach. Additionally, the results show that grain-size is inversely correlated with channel width, but that this relationship is strongest for patches located at bar heads. These findings indicate that systematic patterns are modulated by local processes such as hydraulics or sediment supply, and that the application of downstream fining models may have limited application on the Upper Sandy River at scales finer than a few kilometers.

CURRICULUM VITAE

NAME OF AUTHOR: Eric Steven Levenson

GRADUATE AND UNDERGRADUATE SCHOOLS ATTENDED:

University of Oregon, Eugene
Bowdoin College

DEGREES AWARDED:

Master of Geography, 2021, University of Oregon
Bachelor of Arts, 2015, Bowdoin College

AREAS OF SPECIAL INTEREST:

Fluvial Geomorphology
Hydrology
Remote Sensing

PROFESSIONAL EXPERIENCE:

Graduate Employee, University of Oregon, 2019-present
Math and Human Ecology Teacher, The Sage School, 2016-2019
Math Teaching Fellow, Maine Coast Semester, 2015-2016

GRANTS, AWARDS, AND HONORS:

Rippey Award, University of Oregon Department of Geography, 2020
Sarah and James Bowdoin Scholar, Bowdoin College, 2015
Riley Research Award, Bowdoin College Department of Anthropology, 2014

ACKNOWLEDGMENTS

This thesis is the result of contributions and support from many people within and outside of the University of Oregon Geography Department. My advisor Mark Fonstad and committee member Patricia McDowell encouraged my curiosity about rivers and taught me what it takes to conduct actual research that can make a small contribution to the river science community. They have been patient with my progress and continue to challenge me to pull my head out of the clouds and maintain an attachment to the physical processes in rivers that define our research topics. I benefited from the support and inspiration from my fellow graduate students and postdocs within the River Research Group: Aaron Zettler-Mann, Nicole Merrill, Dion Webster, Devin Lea, Matthew Goslin, and Dakota Whitman. Thank you to my parents and my partner Katie Brady for supporting my transition back to school from my teaching career. I also need to acknowledge the rivers and mountains throughout New Hampshire, Maine, Idaho, Alaska, and Oregon that have captured my attention and energy and inspired me to seek understanding. Lastly, thank you to those who have taught me that getting in the river to play in the turbulence is the most fantastic and profound way to waste some time.

TABLE OF CONTENTS

Chapter	Page
I. INTRODUCTION	1
1. Introduction	1
2. Research Questions	3
II. A METHODOLOGICAL FRAMEWORK FOR IMAGE-BASED GRAIN-SIZE MAPPING	5
1. Introduction	5
2. Grain-Size Mapping Case Study: Upper Sandy river	8
2.1. Surveying Approaches.....	9
2.2. Photosieving: Image-Based Grain-Size Measurement	11
2.2.1. Photosieving Comparison: PebbleCounts and SediNet.....	12
2.2.2. PebbleCounts and SediNet Comparison: Results	13
2.2.3. SediNet Introduction.....	14
2.2.4. PebbleCounts and SediNet Comparison: Results	16
2.2.5. PebbleCounts and SediNet Comparison: Discussion	18
2.2.6. Grain-Size Percentiles.....	19

Chapter	Page
2.3. Geographic Representation.....	22
3. Outcomes.....	26
4. Discussion	29
4.1. Limitations	29
4.2. Advantages	30
4.3. Future Directions	31
5. Conclusion	31
III. SOURCES OF COARSE SEDIMENT GRAIN-SIZE VARIABILITY ALONG THE UPPER SANDY RIVER.....	33
1. Introduction	33
1.1. Implications of Multiscale Grain-Size Mapping.....	34
2. Methods: Grain-Size Map Production	36
2.1. Study Area.....	36
2.2. Image Acquisition.....	38
2.3. Obtaining Image Location and Resolution	39
2.3.1. Structure from Motion Processing.....	40
2.3.2. Image-scale Calculation	40
2.4. Grain-Size Attributes	41

Chapter	Page
2.5. Geographic Attributes	41
2.5.1. River Scale Locational Attributes: Channel-fitted Coordinate System	42
2.5.2. Bar Scale Locational Attributes.....	43
2.6. Morphological Attributes	44
2.6.1. Active Channel Width.....	44
2.6.2. Slope	46
2.7. Multiscale Grain-Size Map.....	49
3. Grain-Size Sorting	50
3.1. Downstream Grain-Size Variability.....	51
3.2. Bar Scale Variability	54
3.3. Morphological Sources of Grain-Size Variability	58
4. Discussion	59
4.1. Surveying Limitations and Advantages	59
4.2. Downstream Grain-size Variability.....	60
4.3. Bar Scale Variability	62
4.4. Grain-Size Association with Active Channel Width.....	63

Chapter	Page
5. Conclusions.....	65
IV. CONCLUSIONS	66
REFERENCES CITED	68

LIST OF FIGURES

Figure	Page
1. Grain-size mapping methodological framework components.....	8
2. Subset of images for photosieving comparison.....	14
3. Stock SediNet model training and testing by grain-size percentile	16
4. Pebblecounts and SediNet photosieving comparison	17
5. Effect of low-end truncation on PebbleCounts performance	19
6. PebbleCounts outputs and master grain-size matrix	20
7. Comparison of image resolution from varied flying heights	22
8. Comparison of UTM and channel-fitted coordinates.....	25
9. Bar scale geographic attributes.....	25
10. Grain-size map production steps.....	28
11. Study Site	38
12. Sandy River hydrograph for water year 2020.....	39
13. Active channel width transects	45
14. Active channel width interpolation diagram	46
15. Comparison of manually digitized and DEM-derived centerlines.....	48
16. Longitudinal profile	48

Figure	Page
17. Multiscale grain-size information in the upper Sandy River	50
18. Comparison of D_{84} histograms in millimeters and psi	51
19. Median grain-size vs. downstream position	53
20. Correlogram of median grain-size at various downstream lags	53
21. Bar scale grain-size sorting.....	55
22. Variability among bar scale grain-size distributions.....	55
23. Histogram of the channel width at each grain-size sample location	57
24. D_{84} vs. active channel width and downbar position.....	58
25. Grain-size response to downstream position and channel width	58

LIST OF TABLES

Table	Page
1. Subset of published approaches to image-based grain-size mapping	7
2. Geographic attributes and their associated spatial scale.....	23
3. Grain-size dataset attribute descriptions.....	27
4. Geographic attributes on the upper Sandy River grain-size dataset.....	42
5. Attribute descriptions for the upper Sandy River grain-size dataset	49
6. Statistical descriptions of downbar sorting	56

CHAPTER I

INTRODUCTION

1. Introduction

Alluvial river forms such as channel geometry and planform are the product of sediment that has been mobilized, transported, and deposited by the river itself. The river morphodynamics paradigm describes interactions between alluvial river morphology and sediment dynamics as a feedback cycle: channel morphology influences the flow hydraulics of moving water; flow hydraulics drive the erosion and deposition of bed material; bed material transport in turn shapes channel morphology (Church and Ferguson, 2015). Given this relationship, the size of sediment grains and their spatial distribution are fundamental metrics for many research topics in fluvial geomorphology such as sediment transport (e.g. Paola and Seal, 1995), flow resistance and velocity (e.g. Lee and Ferguson, 2002), channel geometry (e.g. Dade, 2000) salmonid habitat suitability (e.g. Kondolf and Sale, 1993), and morphodynamic model calibration (e.g. Van De Wiel et al., 2007).

The patterns and processes of fluvial grain-size sorting operate at spatial scales ranging from the river's entire longitudinal profile to small clusters of grains (Powell, 1998). At the scale of a few individual grains, size-dependent differences in inertia lead to pebble clusters when a single immobile clast encourages an upstream deposit of coarse bedload and a downstream deposit of fine material (Richards and Clifford, 1991). Channel width scale bedforms, such as a gravel bar, exert topographic control over the flow structure leading to sediment sorting (Ashworth, 1996). At the channel length scale of an entire stream or river, the exponential downstream decrease in grain-size arises from size selective transport and abrasion processes. The interdependencies among the patterns and processes of sediment sorting across these spatial scales are poorly understood (Powell, 1998) despite the importance of the distribution of sediment for shaping channel morphology, flow hydraulics, and sediment transport regimes. Recent efforts to develop image-based remote sensing solutions for measuring sediment grain-sizes (i.e. photosieving) present an opportunity to advance our understanding of sediment

sorting across spatial scales and its relationship to channel morphology. However, the growing collection of photosieving methodologies and software products remain largely in the development and ‘proof-of-concept’ stages due to uncertainty surrounding the key methodological choices and their implications.

Overcoming these barriers to map river morphological parameters, such as grain-size, at high resolutions and across large extents is growing research field due to the implications for our basic understanding of fluvial forms and processes. Carbonneau et al. (2012) argued that traditional widely spaced surveys have led to a focus on averages and trends rather than heterogeneity in river morphology. Drawing from landscape ecology theory, they argue for a representation of riverscapes as a combination of broad and local scale trends marked by discontinuities and heterogeneity. Many conceptual frameworks for relating systematic trends and local discontinuities were conceived based on traditional observations of river environments. For example, the River Continuum Concept (Vannote et al., 1980) and the Process Domain Concept (Montgomery, 1999) hypothesize how local river dynamics emerge from coarser scale processes. Developing and applying riverscape mapping strategies provides an opportunity to evaluate these conceptual frameworks (e.g. Fonstad and Marcus, 2010) and even construct new theory that explains how systematic patterns emerge from local processes.

Mapping sediment grain-size variability at high resolutions and across a large extent is situated within the riverscape paradigm for its relevance to understanding fluvial form and process. The results of such an effort can also contribute to practical river management issues such as aquatic habitat and channel migration hazards. The residents and river management agencies surrounding the study site – the upper Sandy River in Oregon, USA – is particularly interested in the hazards and aquatic habitat produced by the natural dynamics of the upper Sandy River. The upper Sandy River’s path begins on the glaciers of Mt. Hood in the Oregon Cascades before traveling approximately 90 kilometers to the northwest where it joins the Columbia River. Glaciers carved the Sandy River valley from volcanic bedrock, and the current state of the watershed is the result of deposition of volcanic material over the past 1,700 years and subsequent surface erosion (Handelman et al., 2014). Lahar events have deposited highly erodible sediment within

the channel and along the valley bottom. The combination of steep terrain, abundant sediment, and flooding contributes to a dynamic channel that frequently migrates laterally.

Major flooding events in 1964, 1996, and 2011 caused channel migration that destroyed private and public property. In response to the 2011 40-year flood, the Sandy River Watershed Council has spearheaded a restorative flood response plan that focuses on restoration actions to mitigate channel migration hazards while improving aquatic habitat for salmonids. Many of the proposed river management interventions, such as levee deconstruction or side-channel reconnection, function by imposing certain morphologic conditions in hopes of producing desirable river states and processes into the future. These applications motivate the continued development of our understanding of the relationship between fluvial forms and processes. The consequences of management interventions that are out of step with river behavior are exemplified by the flood risk mitigation efforts in the 1960s on the upper Sandy River that rechannelized the river and stabilized banks with levees. Today, many of the restoration actions are undoing these earlier projects that increased channel conveyance and prevented the more frequent and smaller magnitude channel adjustments that serve to dissipate the river's energy during floods. These management issues in the upper Sandy River are fundamentally linked to sediment patterns and processes as well as an understanding of river behavior that embraces the combination of large and local scale form and process. This examination of the spatial patterns of sediment grain-size may be useful for practitioners and managers in the upper Sandy River as they seek context for specific restoration locations within the larger river system.

2. Research Questions

This research aims firstly to address the current barrier facing researchers and practitioners who may benefit from image-based grain-size measurement techniques by introducing a methodological framework that describes the principal components of photosieving approaches and the aspects of the resulting grain-size data products that are influenced by methodological choices. The second objective of this study is to apply this

methodological framework to map the variability of coarse sediment within the upper Sandy River, Oregon, USA, analyze the results in relation to channel morphology, and discuss the results in the context of local controls and systematic patterns. These research objectives are guided by the following research questions:

1. Which existing image-based grain-size measurement methods will enable locally accurate and precise grain-size observations across a large extent?
2. What are the sources of coarse grain-size variability at patch, bar, and river segment scales along the upper Sandy River?

CHAPTER II

A METHODOLOGICAL FRAMEWORK FOR IMAGE-BASED GRAIN-SIZE MAPPING

1. Introduction

Significant research energy has been dedicated to developing image-based solutions for measuring sediment grain-sizes (i.e. photosieving) in order to reduce the labor associated with traditional measurements (e.g. Wolman, 1954; Bunte and Abt, 2001) and enable grain-size mapping over larger extents. Grain-size remote sensing thus far has largely remained in the methods development and ‘proof-of-concept’ stages of research. The result has been a multitude of photosieving methodologies and software products – each of which has only seen a handful of applications. Each of these image-based grain-size mapping techniques applied to the same study area will lead to distinct grain-size datasets due to the variation in their range of measurable grain sizes, precision, accuracy, spatial coverage, equipment cost, fieldwork, and software requirements. Currently, river researchers who may benefit from the efficiency and coverage afforded by these procedures are left without a structure for evaluating each photosieving method’s suitability for specific research objectives. The aim of this article is to provide a model for aligning methodological choices within the photosieving chain of production with pre-defined research objectives.

This work presents a methodological framework that describes the main components of image-based grain-size mapping approaches and the aspects of the resulting grain-size data products that are influenced by methodological choices. I apply this framework to a case study on the upper Sandy River in order to facilitate a combination of literature reviews and quantitative analyses of photosieving methodologies and their implications for specific research applications. Sediment grain-size and its distribution throughout the river system is a fundamental metric for many research topics in fluvial geomorphology such as sediment transport (e.g. Paola and Seal, 1995), flow resistance and velocity (e.g. Lee and Ferguson, 2002), channel geometry (e.g. Dade, 2000) salmonid habitat suitability (e.g. Kondolf and Sale, 1993), and

morphodynamic model calibration (e.g. Van De Wiel et al., 2007). The variety of data requirements among these research topics as well as the continued development of photosieving methods motivates the methodological framework and case study approach used here.

All image-based methods for grain-size mapping consist of three fundamental components: (a) surveying and image acquisition, (b) photosieving (i.e. estimating grain-sizes from images); and (c) geographic representation. Note that the term ‘photosieving’ is often used as shorthand for the entire process of producing a grain-size map using imagery, however photosieving moving forward refers specifically to extracting grain-size information from images. Image acquisition strategies in previous studies range from helicopter-based aerial surveys, handheld images of 1 m² extents, and orthomosaics of gravel bars produced through structure from motion (SfM) photogrammetric processing of drone-based images (Carbonneau et al., 2004; Chardon et al., 2020; Fonstad and Zettler-Mann, 2020). Existing photosieving techniques vary from manual measurements of grains in photographs to fully automated algorithms for estimating either grain-size distribution percentiles or the size of individual grains. Geographic representation emerges as a third component because the utility of grain-size results depends upon descriptions of the grains’ locations. Geographic topological attributes for grain-size mapping are most commonly described as distance downstream in studies of downstream fining, however this single metric fails to describe sample locations at local scales. In this article, I propose a more robust method and some automated tools for improving the geographic representation of image-based grain-size measurements. Table 1 shows a subset of the previously used methods for each of these three components. This framework does not provide a comprehensive summary of existing methods, but instead aims to enable deliberate choices for each of these three components by identifying the overarching differences and implications among existing approaches.

The data requirements for image-based grain-size measurement applications will drive the methodological decisions for the three components listed above. The specific data characteristics that are directly influenced by surveying, photosieving, and geographic representation methods include: (i) the range of measurable grain-sizes; (ii)

the error present in grain-size measurements; (iii) whether information regarding individual grains is retained; and (iv) the spatial scales of interest. Figure 1 delineates which of the steps in data production affect each of these data requirements. The connections between data requirements and framework components are governed by overarching commonalities among contemporary photosieving approaches such as the inverse relationship between image resolution and spatial extent, and the correlation between precision of photosieved grain-size measurements and image resolution. The specifics of these connections are discussed below in Section 2.

Table 1: A subset of published approaches to the three principal components of image-based grain-size mapping.

Task	Method	Citation
Surveying and image-acquisition	Handheld cameras	Piegay et al., 2020
	Drone-based orthomosaics	Fonstad and Zettler-Mann, 2020
	Drone-based non-orthorectified images	Carbonneau et al., 2018
	Helicopter-based non-orthorectified images	Carbonneau et al., 2004
Photosieving	Manual	Adams, 1979
	SediNet	Buscombe, 2020
	PebbleCounts	Purinton and Brookhagen, 2019
	BaseGrain	Detert and Weitbrecht, 2013
	GrainNet	Lang et al., 2020
	Semivariance	Carbonneau et al., 2004
	Autocorrelation	Buscombe, 2008
Geographic Representation	Distance downstream	Zettler-Mann and Fonstad, 2020
	Downbar position	Rice and Church, 2010
	Raster cells	Carbonneau et al., 2004

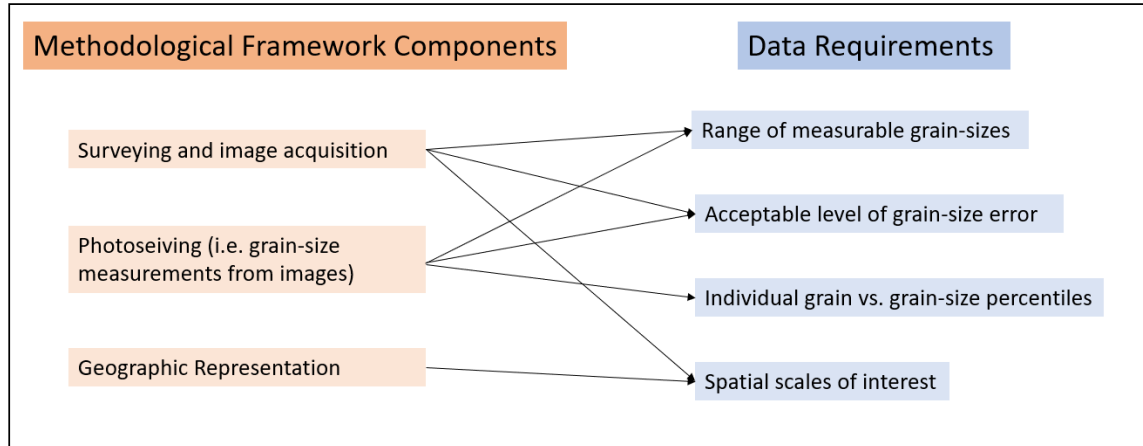


Figure 1: The three components of producing a grain-size dataset and the characteristics of the data product that are influenced by these methodological choices.

2. Grain-Size Mapping Case Study: Upper Sandy River

The remainder of the article is organized to produce a single configuration of pre-existing approaches to the principal tasks of grain-size mapping – surveying, photosieving, and geographic representation – for a case study on the Upper Sandy River in Oregon. The case study’s overarching research objectives are translated into grain-size data requirements, which guide a combination of literature and quantitative analyses in support of decisions for each of the components of image-based grain-size mapping.

The Upper Sandy River in Northwest Oregon is a wandering gravel bed river in which gravel bar development commonly leads to channel migration and avulsions. Mapping the distribution of coarse alluvial grains throughout the river system is important for characterizing the spatial patterns of channel morphology and development, as well as the relationship between patterns and processes of sediment sorting across spatial scales ranging from a few grains to the channel length. The overarching objective is to produce a multi-scale map of coarse sediment grain size that resolves sediment sorting patterns from the patch to river segment scale. Such a dataset would enable analyses of the interdependencies among the scales of sediment sorting and their relationship to channel morphology. Therefore, the decisions for surveying, photosieving, and geographic representation are based on the following research criteria: (i) Capability in capturing the spatial distribution of exposed coarse sediment (b -axis ≥ 16 mm) at patch,

bar, and channel length scales; (ii) *B*-axis estimates within 10% of the actual length and a standard deviation of errors of 1 cm or less; (iii) Applicability to complex river environments characterized by a mosaic of exposed sediment, vegetation, and water surface; and (iv) Efficient and cost-effective grain-size surveying and measurement. The following sections seek an answer to the following question: *Which existing image-based grain-size measurement methods will enable locally accurate and precise grain-size observations across a large extent?*

2.1. Surveying Approaches

Producing a multi-scale grain-size map on the Upper Sandy River presents a significant surveying challenge related to accessing exposed sediment patches throughout the river system. Traditional surveying and measurement approaches such as the Wolman pebble count or grid sampling are far too labor intensive for multi-scale analysis across large extents, however a solution may exist within the increasing number of remote sensing techniques for measuring surface grains. This study focuses on image-based surveys of sediment grains because cameras are a cost effective, widely available, and easily deployable survey tool in comparison to alternatives such as Terrestrial Laser Scanners and LiDAR.

Defining a survey approach depends on a few basic commonalities among contemporary photosieving techniques: (i) Grain-size is first measured in pixels and converted to a metric unit using the known image scale (i.e. cm/pixel); (ii) The precision and accuracy of the grain-size measurements increases with image resolution; (iii) The size of the smallest measurable grain decreases as image resolution increases; (iv) The spatial extent of an image decreases as its resolution increases for a given camera. Given these commonalities, the required image resolution will depend on the portion of the grain-size distribution of interest and acceptable level of error for the end user. Although image resolution requirements vary, all image-based surveys must provide accurate geographic locations of the grains of interest and an accurate image scale to convert pixels to metric units.

Orthoimages are an obvious choice to meet the location and resolution

requirements, and they have been used previously in grain-size mapping efforts (Fonstad and Zettler-Mann, 2020; Zettler-Mann and Fonstad, 2020). Direct georeferencing (DG) of structure from motion (SfM) photogrammetry using drone images and the onboard GPS enables efficient production of orthomosaics without the need for collecting ground control points – an expensive and time-consuming process (Carbonneau and Dietrich, 2017; Carbonneau et al., 2018). However, orthomosaics are associated with blurring effects and require a large number of images to achieve an image resolution comparable to undistorted non-orthorectified images. Fonstad and Zettler-Mann (2020) faced challenges at the photosieving stage of this approach on the Lower Sandy River as downstream fining led to grains that were not consistently resolvable in their orthomosaics.

Carbonneau et al. (2005) collected aerial imagery from helicopters and conducted extensive ground surveys to georeference the non-orthorectified images with resolutions of 3 cm/pixel and 10 cm/pixel. They limited their analysis to areas of continuous exposed gravel and created a statistical relationship between ground truth samples and quantitative image properties including texture and semivariance, which was only successful for the 3 cm images. This approach has the advantage of mapping grain-sizes at the catchment scale, but its uptake by others has been limited due to the high cost of helicopter surveys and the extensive fieldwork involved in collecting ground control points and ‘truth’ grain-size distributions. On the opposite end of the spatial extent spectrum, Chardon et al. (2020) used a handheld camera to collect high resolution images of 1 m² areas with pixel ranges from 0.18 mm to 0.30 mm, but this was limited to 20 images in total.

These existing methods either focus on obtaining high resolution imagery to photosieve local areas with acceptable accuracy and precision (Chardon et al., 2020), or collecting lower resolution imagery to estimate grain sizes across larger extents (Carbonneau et al., 2004; Carbonneau et al., 2005). Obtaining high precision measurements across large extents therefore requires either automating the application of high-resolution image collection and photosieving methods, or decreasing the cost and error associated with coarse scale approaches.

Carbonneau et al. (2018) presented a proof-of-concept for ‘robotic photosieving’ – an alternative that uses drone-based images and a directly georeferenced SfM workflow to efficiently acquire near ground, high resolution, non-orthorectified images and enable calculations of their image scale and locations. They show that the image scale of near-ground non-orthorectified images can be predicted within 3% without the need for ground control or scale objects. The objective of their workflow is to calculate precise camera locations and altitude above ground level (AGL) of near ground non-overlapping images to be used for photosieving by combining them with overlapping imagery from higher altitudes AGL. This process has the added benefit of producing orthomosaics and DEMs, although the topography is not survey grade (Carbonneau and Dietrich, 2017).

Robotic photosieving has a number of advantages for multi-scale grain-size mapping on the Upper Sandy compared to the other surveying methods. First, the drone surveys are very efficient because they do not require ground control points and the resolution of the orthomosaics does not affect the photosieving results. Second, measuring finer grains is possible using high resolution non-orthorectified images compared to the orthomosaics. Third, this workflow provides insurance in the form of orthomosaics that can also be used for photosieving should there be an issue in calculating the image scale or locating the near ground imagery. Finally, extending this proof-of-concept to a robust mapping effort would represent a major contribution to the river remote sensing field. The default flying height for near ground imagery will depend on the chosen photosieving method and its minimum number of measurable pixels. In the context of the overarching grain-size mapping framework, the decision to employ robotic photosieving surveys implies the general approach of automating high-resolution local scale methods for the application across large extents.

2.2. Photosieving: Image Based Grain Size Measurement

Obtaining grain-size information from the near ground images through photosieving is now possible given the ability to acquire high resolution images with acceptably accurate and precise GPS coordinates and image scales. This section focuses on navigating the range of photosieving choices for estimating grain sizes from the drone

images.

Manual measurements of surface grains from photographs in the 1970s initiated the development of photosieving. Contemporary photosieving methods generally fall into two categories as they automate the process of either: a) extracting and measuring individual grains, or b) extracting and correlating image statistical properties with the grain-size distribution (Piégay et al., 2020). Applications requiring information at the scale of grains are limited to the photosieving methods that segment individual clasts, such as the PebbleCounts or Basegrain algorithms (Purinton and Brookhagen, 2019; Detert and Weitbrecht, 2013). Many research applications can forego grain-by-grain information and can therefore adopt either grain segmentation or statistical approaches. Carbonneau et al. (2004) provide an early example of the statistical approach using correlations between ground-truth grain-size distributions and the image texture and semivariance of their helicopter-based imagery. The most recent iteration of the statistical approach involves machine learning architectures such as GrainNet and SediNet, which both use convolutional neural networks (CNNs) to extract image properties and predict sediment characteristics – including grain-size percentiles (Buscombe, 2020; Lang et al., 2020). Cases in which the primary objective is to capture the grain-size distribution, it can be derived from either a correlation with image properties such as texture or semivariance, or from the outputs of grain segmentation techniques (e.g. PebbleCounts).

2.2.1. Photosieving Comparison: PebbleCounts and SediNet

PebbleCounts and SediNet represent the cutting edge of these two strains of image-based grain-size measurement techniques. PebbleCounts segments individual grains while SediNet extracts image properties and predicts grain-size percentiles. A comparison of PebbleCounts and SediNet’s photosieving performance for the task of producing a grain-size map on the Upper Sandy River is based on their error in measuring grain-size percentiles for grains over 16 mm, and efficiency when applied to a large number of images. Manual measurements of grain-size *b*-axes in ten images from the Upper Sandy provide the means to evaluate the accuracy of photosieving outputs. The manual measurements are used here to produce a ‘labeled’ dataset, which is analogous to

a ‘truth’ dataset for the purpose of model evaluation. All methods in question – labeling, PebbleCounts, and SediNet – deal with grain size in pixels, which are later converted to metric units using the image resolution.

2.2.2. *PebbleCounts Introduction*

PebbleCounts is an open-source algorithm that uses k -means clustering of both spatial and spectral information to delineate individual grains (Purinton and Brookhagen, 2019). The algorithm begins with a series of pre-processing steps designed to mask shadows, sand, and vegetation. The first step is non-local means denoising of the RGB image, which deals with intra-grain color differences. The RGB image is converted to gray-scale with top-hat, Sobel, and Canny methods to detect edges and preserve inter-grain differences. Following edge detection, the algorithm uses K-means clustering with manual selection (KMS) to segment individual pebbles. The number of clusters begins with 1 and is recalculated with an inertia improvement of 1-10%. This clustering method allows PebbleCounts to accept images with varying number of grains to segment. The algorithm uses a ‘windowing’ approach, which runs the KMS on three scales of the image. This allows the recognition and removal of the largest grains, then intermediate, and finally the smallest resolvable grains. The segmentation approach is naturally limited in its application to sub-pixel grains, whereas SediNet may be capable of predicting sub-pixel grain sizes (Buscombe, 2020).

The PebbleCounts software includes semi-automated and fully automated algorithms designed for the application to orthorectified or regular images at approximately 1 m² scales. Its primary advantage over previously developed watershed segmentation approaches (e.g. BaseGrain) is its potential application in complex settings without ideal interlocking, uniformly colored, and oblate grains (Purinton and Brookhagen, 2019). The example images in Figure 2 show the importance of applicability to complex settings defined by intragranular variability, mixed in vegetation, and sand.



Figure 2: Eight of the ten images used to compare SediNet and PebbleCounts to manually measured grain-sizes.

2.2.3. SediNet Introduction

SediNet is an open-source configurable machine learning framework designed by Daniel Buscombe to extract sediment characteristics from imagery. It uses a convolutional neural network (CNN) to map image inputs to desired outputs, including continuous prediction of grain-size percentiles and categorical prediction of grain shape and color (Buscombe, 2020). The image feature extractor is composed of four convolutional blocks. Each convolutional block includes multiple two-dimensional convolutional filter layers, batch normalization layers, and two-dimensional max pooling layers. A customizable dropout layer after the last convolutional block is used to prevent overfitting, and the outputs of the feature extraction become the inputs of a multilayer perceptron, creating a prediction layer that is run through a linear activation function. Along with the model architecture, SediNet provides a dataset of 409 images with labeled grain-size percentiles and a modular file structure that allows adjustment to the models through a defaults script and configuration file.

SediNet is a framework rather than a single model, and therefore decisions in implementation will impact the resulting model as well as its performance. The set of images used for model training, loss functions, and optimization functions are all easily configurable components of the SediNet framework. In this study, three SediNet implementations are trained and evaluated in comparison to the semi-automated

PebbleCounts algorithm. The first implementation is hereafter referred to as the ‘stock’ model, as it uses the default configuration and training set available through the SediNet Github. The stock model uses a Pinball loss function and a Root Mean Square Propagation (RMSProp) optimization function. Pinball loss is used specifically for calculating quantile loss, which is appropriate for the prediction of nine grain-size percentiles. The RMSProp optimizer is similar to the commonly used gradient descent with momentum, but functions by maintaining a discounted average of the square of the gradients, which is used to normalize the current gradient. The initial learning rate was defined as 0.002 with 5 training epochs. The model was trained on 204 images and tested on 205 before its use to predict on the 10 images from the Upper Sandy.

Figure 3 visualizes the performance of the stock model on the 204 training images and 205 testing images provided with SediNet. Specifically, each individual chart displays one of the nine percentiles predicted by the model. This dataset includes both sand and gravel images with a range of image spatial resolutions. The results indicate that prediction skill degrades for the larger grain sizes within each percentile. Specifically, this appears to include some bias as the predictions are consistently larger than the actual grain sizes.

The second implementation – ‘Gravel1’ – uses the same model architecture, but it is trained on a subset of the training set that only includes images of gravel. Gravel is defined as sediment with at least a 2 mm intermediate axis. The third implementation – ‘Gravel2’ – changes a number of model components and again is trained on only images of gravel. All input features are scaled, and the Pinball loss function is replaced with a mean square error (MSE) loss function. The rationale for this replacement is to deal with the Pinball loss function’s heavy penalization of negative errors in higher percentiles, and positive errors in lower percentiles, which could have contributed to the stock model’s overpredictions of large grains and underpredictions of small grains. The MSE loss function – commonly referred to as L2 loss – computes the sum of squared distances between our target variable and predicted values, which can lead to outsized influence by outliers in the dataset. The RMSProp optimizer is replaced by an Adam optimizer, which uses an adaptive learning rate for each parameter. It maintains an exponentially decaying

average of past squared gradients and past gradients, thus combining features of RMSProp and momentum. The biased predictions were slightly improved in the Gravel 2 model, however all three models struggled to predict grain-sizes with any meaningful accuracy or precision on the labeled dataset.

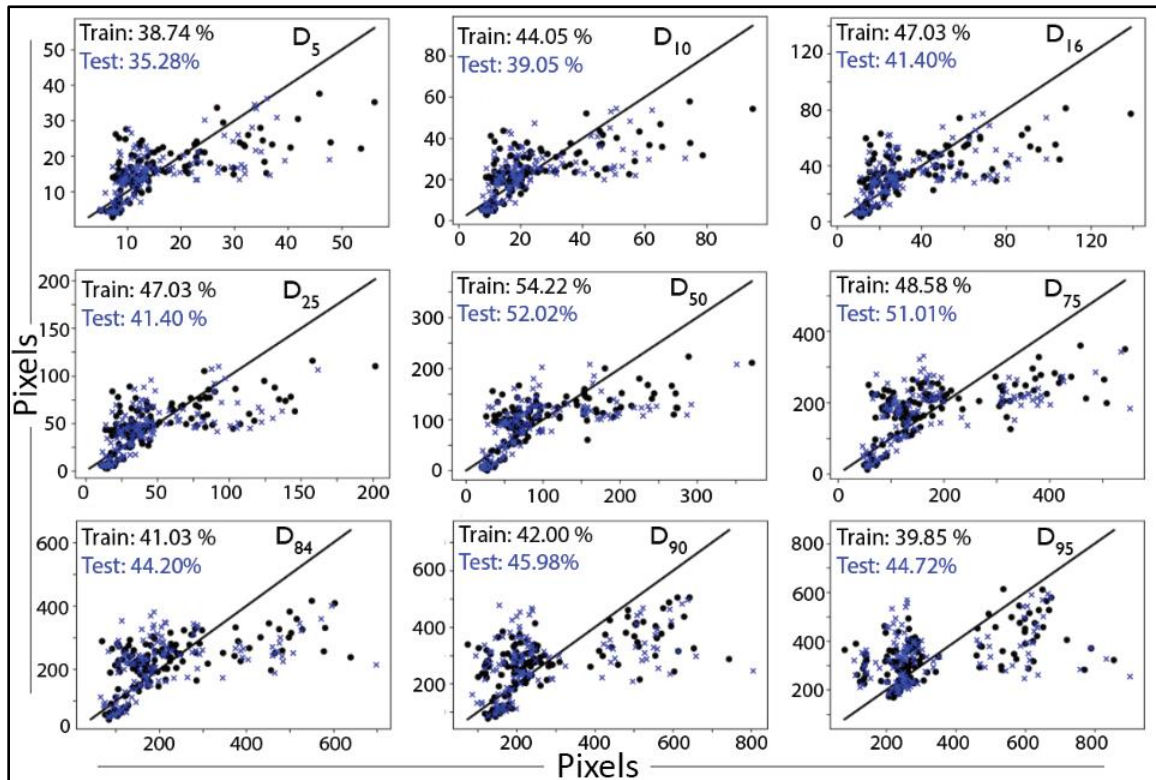


Figure 3: Stock model predicted vs. actual (horizontal axis) grain sizes for each of the nine percentiles on the 204 train images (black) and 205 test images (blue). Prediction skill for the training and testing images is displayed in the upper left of each graph.

2.2.4. PebbleCounts and SediNet Comparison: Results

Grain-size percentiles were calculated from the manual grain-size measurements and PebbleCounts segmentation for each of the ten labeled images from the Upper Sandy to enable comparison with the grain-size percentiles predicted by the three SediNet models.

Figure 3 visualizes each model’s accuracy as percent error for each percentile (mean error divided by the mean b -axis for a given percentile). All three SediNet models displayed inaccurate predictions of the coarse end of the distribution while PebbleCounts was inaccurate in measuring the 5th, 10th, and 16th percentiles. The segmentation

algorithm reliably predicted the D_{50} b -axis within 10% of the labeled length. The precision of each model is not characterized by the errors shown in Figure 4. The standard deviation for PebbleCounts' errors in prediction the median b -axis was 8.27 pixels, which was significantly lower than the SediNet models' standard deviations ranging from 20.3 to 22.5 pixels. This indicates that PebbleCounts is more precise than SediNet above the 25th percentile.

After initial model training, SediNet's application is far more time efficient in comparison to PebbleCounts. Percentiles predictions for an individual image is accomplished in under one second, and this prediction can easily be scaled to a very large number of images. PebbleCounts requires 5-10 minutes per image, and this timeframe includes active participation by a researcher to operate the commandline interface and manually select correctly segmented grains.

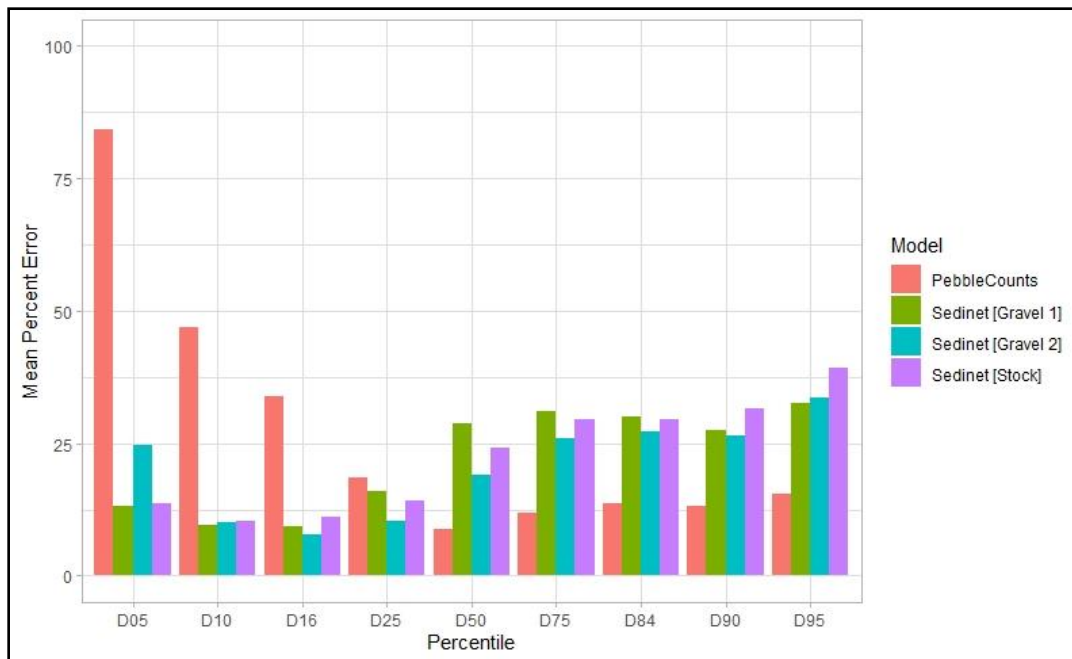


Figure 4: Comparison of the performance of three configurations of the SediNet architecture and PebbleCounts in predicting the grain-size percentiles of 10 manually labeled images. Mean Percent Error is calculated as the RMSE normalized for each percentile's mean value.

2.2.5. PebbleCounts and SediNet Comparison: Discussion

PebbleCounts' poor performance on lower percentiles can easily be explained by its limitation in segmenting grains with b -axes shorter than 20 pixels (Purinton and Brookhagen, 2019), whereas manual measurements can resolve pixels down to a single pixel. PebbleCounts' performance across these low percentiles improves drastically when the labeled dataset is truncated at 20 pixels. Figure 5 shows a comparison of aggregated grain size distributions for the 10 labeled images produced by: (a) manual measurements of b -axes, (b) manual measurements of b -axes with a lower end truncation at 20 pixels, and (c) PebbleCounts photosieving. Visual inspection of the three distributions reveals strong agreement between the PebbleCounts and the truncated labels. It is worth noting that the errors calculated for Figure 3 were for the untruncated labels, which means that the PebbleCounts accuracy is improved following low-end truncation.

The SediNet models' inability to accurately predict the higher percentiles is a more complicated challenge to overcome. A 409 image train and test set is very small for a machine learning model, and the two gravel implementations were trained on an even smaller set. The SediNet models did not see any images from the Upper Sandy during training, and it is reasonable to expect that its performance will improve drastically as the labeled dataset increases in number of images and representation of diverse sedimentological environments. The biased predictions may be attributable to the challenge of calculating quantile loss, and therefore studies that only require a single grain-size metric, such as the D_{50} , may have much greater success in applying SediNet. Another outstanding question in the use of CNNs for photosieving is whether loss functions such as RMSProp or Adam cause overshooting of flat minima and therefore reduce the capacity for the model to generalize to other imagery datasets.

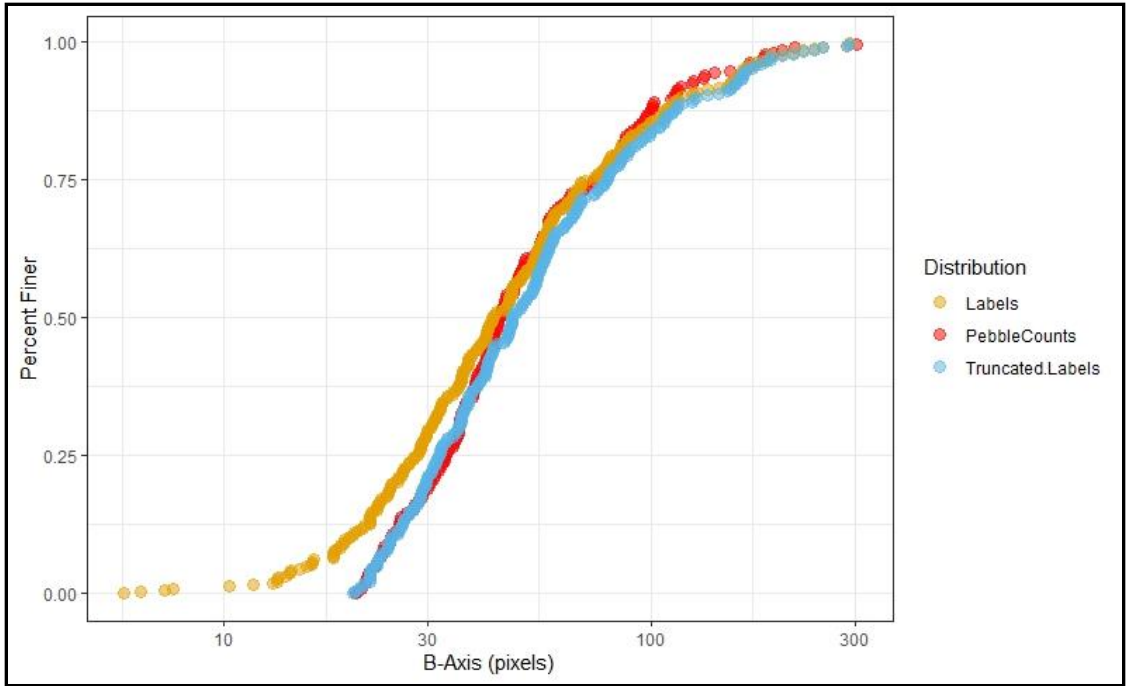


Figure 5: Aggregated grain-size distributions of 10 images from the Upper Sandy. Manual photosieving is shown in orange. Manual photosieving with a low-end truncation at 20 pixel b-axes is shown in blue. PebbleCounts is shown in red.

Based on the results of this comparison and the research objectives focused on characterizing the distribution of coarse sediment, this study moves forward with the PebbleCounts photosieving method. Although SediNet is limited in predicting the larger grain-size percentiles, its efficiency is far superior to PebbleCounts and it is more capable at representing the fine end of the grain-size distribution. A growing labeled dataset and continued refinements to the algorithm indicate that SediNet will be a much more useful tool in future investigations into grain-size variability that do not require grain-by-grain information.

2.2.6. Grain-Size Percentiles

Photosieving in PebbleCounts produces a matrix for each image (i.e. sample) in which rows represent individual grains and columns provide measurements such as *a* and *b* axes measured in both pixels and meters (see ‘PebbleCounts Outputs’ in Figure 6). Comparisons among each of the samples depends upon a common description of the grain-size distribution that can be stored in a single matrix. Grain-size percentiles meet

this requirement, but their calculations require careful consideration of the interactions among the image acquisition process, the limitations of PebbleCounts, and the study objectives. Image-based approaches to measuring grain sizes are all limited in the range of measurable grain-sizes, and this range cannot vary among samples if comparisons are desired (Graham et al., 2010). The low end of the distribution is limited by image resolution, while the coarse end is limited by the area covered in the image. A size-dependent bias in the distribution can result from such limits to the range of measurable grains as the coarsest and finest grains may be undercounted.

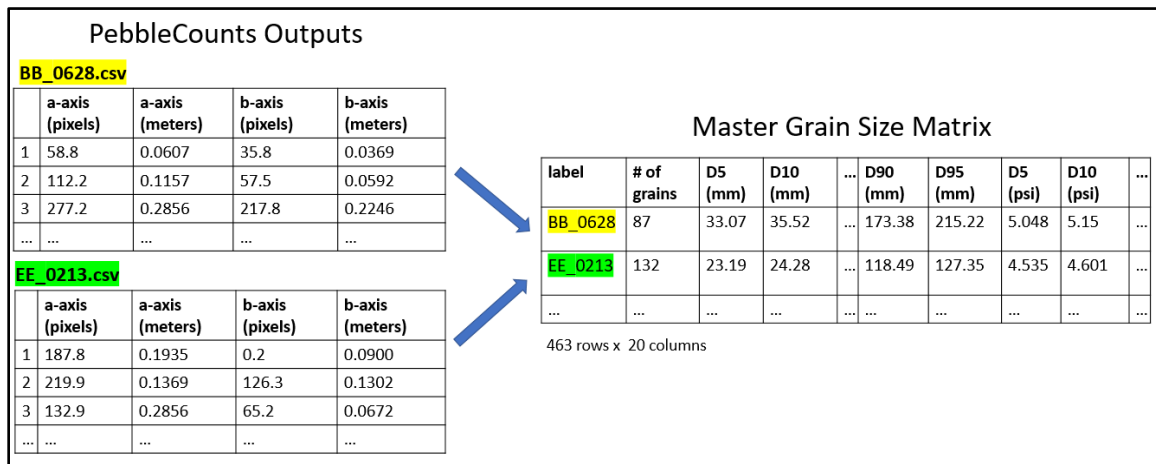


Figure 6: Excerpts from two example outputs from PebbleCounts on the left. Grain-size percentiles are calculated from each of these outputs. Each sample's unique label, number of grains measured, and grain size percentiles become one observation (i.e. row) in the master grain size matrix.

The coarsest grains may not be represented if the sampling area is too small, while the finest grains are certainly not represented if the image cannot resolve individual grains. This size-dependent bias presents a challenge for multi-scale analyses of grain-size as observations of local variability necessitate small sampling areas, but larger sampling areas are needed to represent the population (Graham et al., 2010); a conflict that is exacerbated in river environments such as the Upper Sandy in which the surfaces of gravel bars are mosaics of vegetation, exposed gravel, and sand rather than idealized continuous gravel surfaces. Given this mosaic, researchers generally estimate grain size populations by ignoring smaller patches of exposed sediment in favor of larger sampling locations that provide the areal extent necessary to include the coarsest grains. To deal

with size-dependent bias on the coarse tail of the distribution, I take the alternative approach of sampling small patches to enable examinations of variability at small spatial scales. These patches can be aggregated with nearby samples to represent the grain-size population.

Fine sediment provides a much greater obstacle to representing grain-size distributions through segmentation-based photosieving. The PebbleCounts algorithm reliably measures grains with b -axes of at least 20 pixels (Purinton and Brookhagen, 2019). Purinton and Brookhagen (2019) altered the image resolution within a controlled experiment and showed the predictable result that decreased resolution led to undercounting of fine pebbles.

Figure 7 displays an extreme case of the effect of varying AGL s between two images acquired on the Upper Sandy. Image *A* has an image resolution of 1.1 mm/pixel, while Image *B* has a resolution of 0.3178 mm/pixel. Given the 20-pixel lower cutoff, grains with b -axes longer than 22 mm would be measured for Image *A*, while all grains with b -axes longer than 6.4 mm will be measured in Image *B*. A simple solution is to use a consistent near ground flying height, however bar topography and deviations in flying height due to wind, obstacle avoidance, and errors in the drone's internal GPS introduce deviations in drone AGL and therefore image resolution. Figure 5 in Section 2.3.5 shows that PebbleCounts' precision is improved across the grain-size distribution with the application of a 20-pixel low end truncation. This technique can serve a dual purpose by identifying a metric b -axis length as the threshold for low-end truncation and choosing a default flying height that produces a pixel resolution less than 5% of the metric threshold. For example, the objectives here are to measure grains with a b -axis of at least 16 mm. Given the 20-pixel truncation, the default flying height and camera specifications should therefore produce images with a resolution less than 0.8 mm/pixel.

Following low-end truncation, calculating a percentile from the grain-by-grain data requires interpolating between the two grains on either side of the given percentile. Linear interpolation is limited when applied to classified data measured with sieves or templates, however these issues do not apply to the continuous outputs measured through

photosieving (Graham et al., 2010). Therefore, a simple quantile calculation can be used to calculate the following percentiles: D_5 , D_{10} , D_{16} , D_{25} , D_{50} , D_{75} , D_{84} , D_{90} , D_{95} .

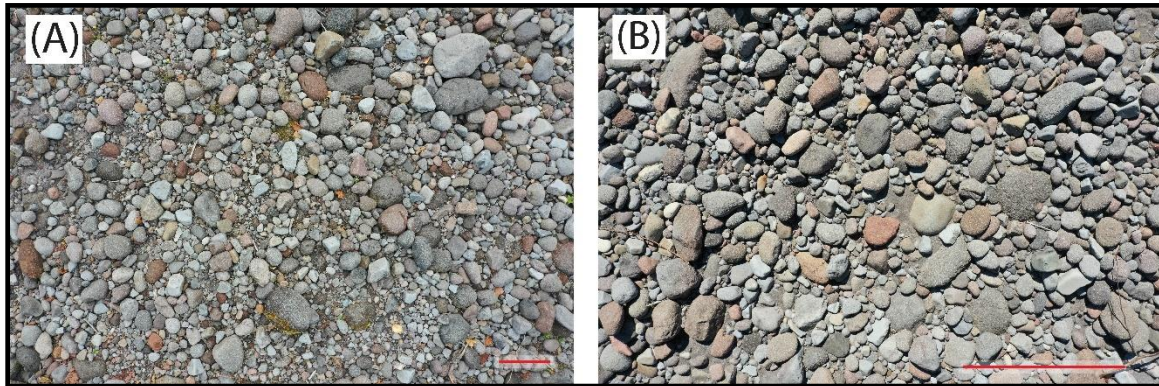


Figure 7: A comparison of images captured from a flying height of 4.258 m (A) and 1.348 m (B). Both images are 3628 x 5472 pixels. The red lines in the bottom right corner each show 500 mm in real-world distance, which reflects differences in image resolution (i.e. mm/pixel). These images were not processed with PebbleCounts and are therefore not included in the grain size mapping analysis.

2.3. Geographic Representation

The photosieving processes described above are not geographical, meaning that the resulting grain-size distributions have no information regarding their location. The objective of this section is to identify geographic attributes that will describe each grain-size distribution's specific location and its spatial relationship to other samples in the dataset. A key challenge is automating the process of calculating these geographic attributes and attaching them to the individual grain-size distributions.

The implication of adopting the robotic photosieving methodology for grain-size surveying is that each near-ground image represents one 'sample,' the location of which is derived from the camera location upon image acquisition. Each image displays grains at the scale of a 'patch,' which has been defined by both spatial scale and bed material composition (Paola and Seal, 1995; Nelson et al., 2014). The term patch is used here to refer to a local spatial scale of approximately 1 m^2 . In this case, the terms 'patch,' 'sample,' and 'near ground image' are analogous and will be used interchangeably based on the context. Although a sample covers an area of approximately 1 m^2 , it may be useful for its geographic location to be represented as a point to enable easy comparisons of

grain-sizes based on sampling location. The point location of the sample can be derived from the camera location obtained through the robotic photosieving workflow. The camera's latitude and longitude approximate the sample's centroid given the understanding that the surveying methods utilize nadir near ground imagery.

Latitude and longitude do not necessarily provide meaningful geographic information for comparing grain-size variability or characterizing the scales of sediment sorting throughout a river system. In order to examine topological relationships among patches at the bar-scale and the river segment scale, locational attributes must represent the sample's location within the gravel bar and within the river system. Table 1 provides a list of quantitative attributes that describe a sample's position at various spatial scales. Global positions (i.e. latitude and longitude) can be projected onto a two-dimensional Cartesian plane, however even Cartesian coordinate systems such as Universal Transverse Mercator (UTM) do not adequately represent a sample's position within a meandering river system.

Table 2: The desired geographic attributes for each grain-size sample and their associated spatial scale.

Attribute	Scale
Latitude	Global
Longitude	Global
X (UTM)	Global
Y (UTM)	Global
Distance Downstream	River
Distance from centerline	River
Bar Name	Bar
Distance Downbar	Bar
Normalized Distance Downbar	Bar
Distance from Bar Edge	Bar

Channel-fitted coordinate systems present a solution at the river scale by describing a sample's location using a streamwise axis (s) based on downstream distance

from a chosen point along the channel centerline, and an axis that is normal (n) to the streamwise axis. Legleiter and Kyriakidis (2006) present the mathematical basis for such a coordinate transformation procedure. Figure 8 provides a reference to compare the Cartesian x and y axes to the channel-fitted s and n axes and how a point's position is described by the two systems.

This channel-fitted coordinate system does not characterize a sample's location within a gravel bar, but it does provide a framework for transforming its UTM coordinates into a bar scale location. Figure 9 shows an example of how the Legleiter and Kyriakidis (2006) transformation can describe point's bar-scale position in terms of its *downbar distance*. *Downbar distance* is calculated by replacing the channel centerline with a bar centerline in the same script. The purple 'Downbar Distance Reference' within Figure 9 provides an example of a manually digitized bar centerline. At this point, determining the position of this line is left to researcher judgement. A sample's distance from the boundary between the exposed bar and the low flow channel can also be obtained by digitizing the bar edge and measuring the shortest Euclidean distance between the sample centroid and the bar edge.

These global, river, and bar scale geographic coordinates enable comparisons of patch-scale grain size distributions at multiple scales. Samples can also be aggregated based on proximity in terms of Euclidean distance, stream normal distance, or bar membership to extend the patch-scale grain size distributions to larger spatial scales. This strategy for representing samples' spatial attributes is essential for investigations into sediment sorting, which inherently ask how grain size responds to geographic position within a given scale. Downstream fining is a familiar example that uses downstream distance as the sole representation of a grain-size sample location, but it ignores remarkable variability and patterning in the distribution of sediment that is often observed within a downstream fining trend due to lateral sediment sources (Rice, 1998) and local variability within gravel bars (Rice and Church, 2010).

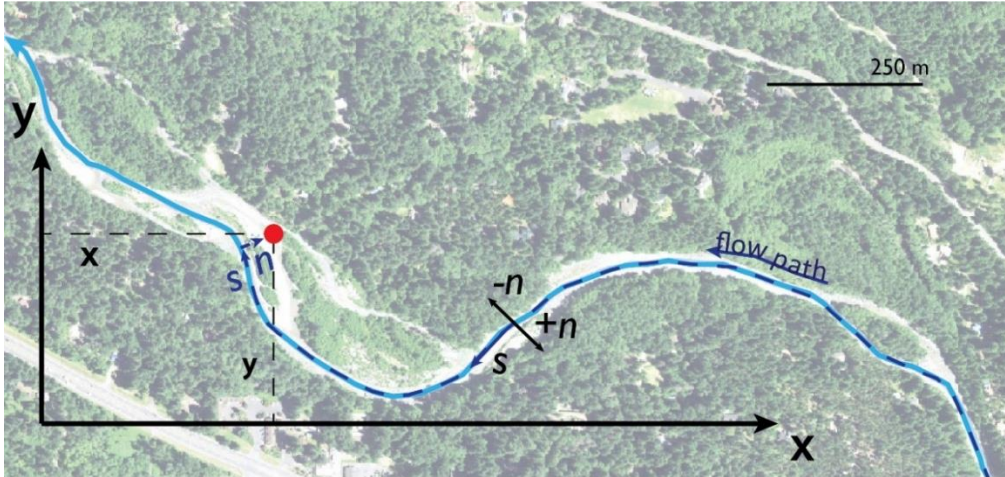


Figure 8: Comparison of Cartesian (x, y) coordinates and channel-fitted (s, n) coordinates adapted from Legleiter and Kyriakidis (2006) and Smith and McLean (1984) shown on a ~ 1.5 km reach within the study site. Flow is from right to left. The dashed lines show the coordinates within each coordinate system for an arbitrary point.

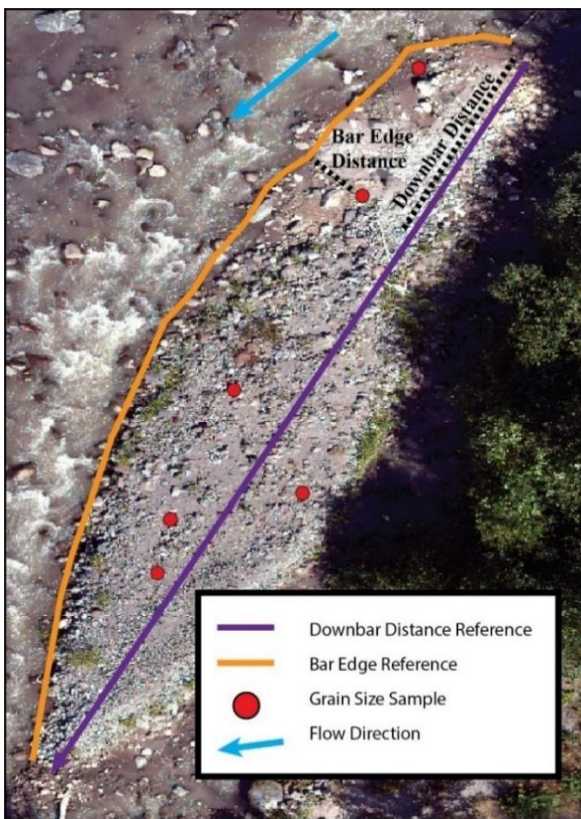


Figure 9: Orthophoto of gravel bar within the study area produced by the drone survey with the associated bar-scale geographic attributes. The dotted black lines are included to conceptualize the measurements of the two principal bar-scale attributes of interest: downbar distance and bar edge distance.

3. Outcomes

Section 2 describes a configuration of a grain-size mapping framework that uses Carbonneau et al. (2017)'s robotic photosieving method for surveying, the PebbleCounts software for photosieving (Purinton and Brookhagen, 2019), and an approach to geographic representation that describes each sample's position within the river system (Legleiter and Kyriakidis, 2006) and gravel bar. The deployment of this methodology would produce a dataset of grain-size samples with the attributes displayed in Table 2, however applying each of these steps to a large number of samples presents a barrier to producing a true multi-scale grain-size map over a large extent. Processing each individual sample through structure from motion, PebbleCounts photosieving, and the numerous geographic transformations restricts the number of total samples – an obstacle that may contribute to the limited adoption of image-based grain-size mapping methods. To address this challenge, a set of tools for automating many steps in the process of producing a grain-size dataset are or will be available through Github. For example, James Dietrich coded the stream normal transformation into a Python script (Dietrich, 2019). Using the UTM coordinates of evenly spaced points along channel centerline to define the streamwise axis, this script efficiently transforms a series of points' (i.e. sample centroids) UTM coordinates to the stream normal coordinate system. This same script can be applied with the bar centerlines to retrieve each sample's downbar distance. I wrote a new open source script that measures this *distance from edge* using the shortest Euclidean distance between the sample centroid and the bar edge. Table 3 describes each step of the mapping process and delineates which steps are automated, semi-automated, or manual. The automated steps are generally in the form of Python scripts available through Github with well-defined input and output files. Although many of these tasks could have been combined into a single script, the step-by-step approach allows others to adapt these scripts to their own tasks and research goals.

Table 3: Descriptions of the attributes produced through the configuration of the grain-size mapping framework presented in Section 2.

Attribute	Description
Label	Unique to each sample based on bar name and original image file.
Grain-Size Percentiles (mm)	D ₅ , D ₁₀ , D ₁₆ , D ₂₅ , D ₅₀ , D ₇₅ , D ₈₄ , D ₉₀ , D ₉₅ calculated from PebbleCounts outputs with a 16 mm lower truncation
Grain-Size Percentiles (psi)	D ₅ , D ₁₀ , D ₁₆ , D ₂₅ , D ₅₀ , D ₇₅ , D ₈₄ , D ₉₀ , D ₉₅ calculated from PebbleCounts outputs with a 4 psi lower truncation
Latitude	GPS coordinates exported from Agisoft Metashape
Longitude	GPS coordinates exported from Agisoft Metashape
X	Location coordinates projected to the UTM coordinate system
Y	Location coordinates projected to the UTM coordinate system
Bar	Delineates the bar from which the sample was obtained
Distance Downstream (m)	Distance in meters downstream along the channel centerline from the upstream boundary of the study area
Cross Stream (m)	Distance from the channel centerline
Distance Downbar (m)	Distance in the downstream direction from the bar head
Distance from Edge (m)	Shortest distance from the bar edge

Grain-Size Map Production Steps		
Color Legend		
Manual: Step must be performed entirely by a researcher	Automated: Step can be performed entirely by open-source scripts	Semi-automated: Step requires a researcher to operate tools.
Objective	Inputs	Outputs
Acquire Images	Fieldwork	JPEG images organized based on gravel bar membership
Rename image files to: a) include bar name b) give each image a unique name	A folder containing subfolders for each bar containing corresponding image files	Renamed files. Example: 'DJI_0001' → 'C_DJI_0001'
SfM to create orthophotos and DEMs of each bar; corrected camera locations	Geotagged images acquired in the field.	Orthomosaics and DEMs stored as GeoTIFFs; camera locations stored as xml files.
Extract the corrected camera locations from SfM processing into a usable format	Folder of xml files containing camera location information exported from Agisoft Metashape	'Master Matrix' in which each row includes an image label, bar name, latitude, longitude, elevation stored in a csv file.
Find bar elevations at sampling locations	'Master matrix'; DEMs; Sample DEM rasters at point locations	Datasets of sample labels and corresponding bar elevation stored in csv files
Calculate image resolution; subset high resolution images for photosieving; write PebbleCounts commandline arguments for each image	'Master matrix'; folder of bar elevations at sampling points; camera specifications; empty folder to store high resolution images	Folder of high resolution image jpeg files; unique PebbleCounts commandline arguments
Measure grain-sizes	PebbleCounts commandline arguments and image files	Csv files storing grain sizes measured through PebbleCounts
Calculate grain-size percentiles	'Master matrix' and csv file outputs from PebbleCounts	Grain-size percentiles attached to the 'master matrix'
Map channel centerlines, bar centerlines, and bar edges	Manually digitize and convert to points the channel centerline, bar centerlines, and bar edges	UTM coordinates for: channel centerline; bar centerlines; bar edges
Transform UTM coordinates to channel-fitted coordinates	James Dietrich script; channel centerline; master matrix	Channel-fitted coordinates attached to the master matrix
Separate 'master matrix' into individual datasets for each bar	'Master matrix'; Empty folder to hold bar-scale datasets	Folder containing datasets of grain-size samples for each bar
Calculate downbar distance	Bar-scale matrix; bar centerline UTM coordinates	Downbar distance attached to bar-scale matrices
Calculate distance from bar edge	Bar-scale matrix; bar edge UTM coordinates	Bar edge distance attached to bar-scale matrices
Combine bar-scale datasets back into a 'master matrix'	Folder containing bar-scale datasets in csv format	'Master matrix'
Measure active channel widths vs. downstream distance	NAIP Imagery, channel centerline	Active channel width vs. downstream distance dataset
Calculate active channel widths for every sample	'Master matrix'; active channel width matrix	Active channel width attached to master matrix
Create longitudinal profile	Channel centerline, LiDAR DEM	Elevation vs. downstream distance dataset
Calculate slope for every sample	'Master matrix'; long profile	Slope attached to master matrix

Figure 10: Steps required to produce a dataset of point locations with GSDs, geographic, and morphological attributes. Colors represent manual, automated, and semi-automated steps.

4. Discussion

The motivation for measuring grain sizes is a first order determinant of the limitations, advantages, and applicability of this grain-size mapping methodology. Research objectives drive decisions regarding the grain-size sampling strategy in terms of sample topological relationships and spatial extent, as well as the within-sample measurement of the grain-size distribution. For example, a particular project's research impetus will determine whether excluding fine grains is appropriate or if measuring surface grains is sufficient. Ideally, a single grain-size map can serve any research question. The map presented here does not meet this goal, however the multi-scale map production strategy and individually automated tools (Figure 10) can serve the continued development towards this objective. At this point, a universally-applicable grain-size map may be out of reach, but a configurable mapping methodology to meet a variety of research objectives is still useful.

4.1. Limitations

Photosieving in general presents some shortcomings in measuring within sample grain-size distributions, the clearest of which is the restriction to surficial grains. This precludes any studies requiring sub-surface grain size measurements from adopting this approach. For investigations into surficial grain-sizes, the research objectives must be aligned with the chosen photosieving technique. PebbleCounts was deemed suitable here based on the primary interest in coarse grains, however this segmentation approach has a number of downsides. The 20-pixel b-axis cutoff for the smallest measurable grains as well as the 5–10-minute processing time per sample (with researcher involvement) will likely prevent the widespread adoption of PebbleCounts. This cutoff introduces surveying challenges even for studies that are uninterested in the finest grains because higher resolution images are required to measure grains of the same size as statistical photosieving approaches or other segmentation approaches such as BaseGrain.

The lower cutoff is also an issue for studies such as this that seek comparisons among samples with possibly varying image resolutions. This variation leads to differences in the range of measurable grains. This variation in range can be dealt with

using a universal low-end truncation, however low-end truncation modifies the entire cumulative grain-size distribution curve (Bunte and Abt, 2001). Therefore, the application of a low-end truncation must be addressed by future researchers adopting similar methodology or by future users of this dataset. Graham et al. (2010) quantified the effect of lower end truncation and demonstrated that a truncation at 32 mm led to a mean error at the D_{50} of -0.2 phi. This bias may not be acceptable for applications requiring high precision and unbiased grain-size percentiles such as bed-load transport calculations (Reid et al., 1996), or for applications that require information about the finest grains. The effect of truncation on percentiles is deemed acceptable for this study based on the primary goal of comparing variability in the distribution of coarse grains. This effect may actually be advantageous for understanding channel development as it removes the effect of sand deposited over coarse grains during receding flows (Graham et al., 2010).

The sampling strategy used here is another potential limitation depending on research goals. The measurement strategy is restricted to exposed areas and excludes subsurface grains and those positioned within the low flow channel. Second, the direct georeferencing robotic photosieving workflow does not lead to continuous data even for exposed areas. The grain-size measurements are limited to the patches where individual non-overlapping images were acquired in the field. Photosieving orthomosaics could theoretically lead to continuous data at least for gravel bars, but there is a sacrifice in terms of image resolution or surveying time. Many river environments, such as the Upper Sandy, prohibit the collection of continuous grain-size information anyway due to the widespread presence of vegetation on bar tops. Nevertheless, the robotic photosieving workflow is not a route towards the measurement of every sediment grain in the river.

4.2. Advantages

The primary advantage of this approach is its efficiency in collecting a large number of samples distributed throughout a complex river environment. The map product is well-suited for examining how grain-size varies throughout the river system from patch to reach spatial scales, and the ability to automate many of the steps facilitates repeat mapping efforts through time or in new locations. Observing grain-size variability in this

manner can serve modeling and empirically based efforts to further our understanding of channel development and relationships among the patterns of sediment sorting and fluvial processes.

The mapping workflow is easily configurable, meaning that specific steps may be altered to meet varying research goals. The automated tools described in Figure 10 could even be applied to tasks besides grain-size mapping. For example, examinations of the distribution of vegetation throughout a river system could apply the same bar-scale location protocols.

4.3. Future Directions

Advancements to image-based approaches to grain-size mapping should focus on reducing grain-size errors and improving efficiency by integrating the components of the mapping process. The machine learning approach to photosieving will likely produce more accurate and precise models in the near future that are transferrable to a range of sedimentological environments. Studies that are only interested in a single grain-size percentile may be able to immediately adopt SediNet due to the challenges associated with calculating quantile loss and optimizing models for nine percentiles. Another outstanding objective is the ability to reliably and efficiently survey and measure grains within the channel.

Simple tools for measuring grain-sizes integrated into a GIS would surely increase photosieving's uptake by river researchers and managers. An interesting possibility is the combination of photosieving with land cover classification algorithms to create a continuous raster model of channel and floodplain surface material that includes grain-sizes for the cells classified as exposed sediment. The ability to produce such a model would be valuable for morphological change detection and could be combined with topographic surveys and hydraulic models to more fully capture the relationship between the erosional forces and boundary resistance that shapes fluvial environments.

5. Conclusion

Image-based remote sensing of fluvial grain-sizes has the potential to dramatically

improve researchers and practitioners access to grain-size information. This article presented a framework that deconstructed these image-based methods into three principal tasks: surveying, photosieving, and geographic representation. Comparisons among existing approaches to accomplishing these tasks was guided by a case study seeking observations of coarse sediment grain-sizes at patch, bar, and river segment scales on the upper Sandy River. The result was a proposed methodology that uses drone-based surveys to acquire near ground non-orthorectified images and derive their accurate locations and image-scales through a directly georeferenced SfM workflow. These images are then processed through PebbleCounts to obtain grain-size information. River-scale and bar-scale geographic attributes are attached to each sample through a set of automated tools. This undertaking represents a step in the progression from methods development efforts to photosieving's role as a useful tool for a wider range of river scientists.

CHAPTER III

SOURCES OF COARSE SEDIMENT GRAIN-SIZE VARIABILITY ALONG THE UPPER SANDY RIVER

1. Introduction

The patterns and processes of fluvial grain-size sorting operate at spatial scales ranging from the river's entire longitudinal profile to small clusters of grains (Powell, 1998). At the scale of a few individual grains, size-dependent differences in inertia lead to pebble clusters when a single immobile clast leads to an upstream deposit of coarse bedload and a downstream deposit of fine material (Richards and Clifford, 1991). Channel width scale bedforms, such as a gravel bar, exert topographic control over the flow structure leading to sediment sorting (Ashworth, 1996). At the channel length scale of an entire stream or river, the exponential downstream decrease in grain-size arises from size selective transport and abrasion processes. The interdependencies among the patterns and processes of sediment sorting across these spatial scales are poorly understood (Powell, 1998) despite the importance of the distribution of sediment for shaping channel morphology, flow hydraulics, and sediment transport regimes.

Our limited ability to observe grain-size patterns across these spatial scales is an obstacle to the continued development of our understanding of their relationships with other morphological descriptors such as channel width and slope. Traditional surveying methods such as Wolman counts provide detailed information about grain-sizes in a particular location, but the labor requirements prevent the use of field surveys for producing multiscale grain-size datasets capable of revealing interactions among the scales of sediment sorting. Recent advancements in grain-size remote sensing techniques present an opportunity to collect sedimentological information from the patch to river segment scale (see Chapter 2). Below, I argue that these innovations in grain-size data collection are tied to opportunities to advance our explanations of the physical processes of sediment transport as well as our conceptual frameworks for relating local to catchment scale geomorphic information. Next, I present a multiscale grain-size map on a 12 km segment of the upper Sandy River in Oregon, USA and answer the following

research question: *What are the sources of grain-size variability at patch, bar, and river segment scales along the upper Sandy River?*

1.1. Implications of Multiscale Grain-Size Mapping

Previous research relating downstream fining with physical explanations of sediment transport provides a useful example of the potential for grain-size patterns at one scale (i.e. channel length) to improve our understanding of fluvial processes. A prominent physical explanation for the relationship between sediment grain-size and entrainment is the equal mobility hypothesis, which is based on field observations and quantitative models. Equal mobility states that all grain-sizes within a mixture are transported at the same rate (Parker and Klingeman, 1982; Parker and Dhamothoran, 1982), which is contrary to size-selective transport in which finer grains are more easily transported than coarser grains. The ensuing debate regarding equal mobility versus size-selective transport led to the recognition that many observed downstream fining rates cannot be explained by abrasion alone – a strong argument against the equal mobility hypothesis (Powell, 1998).

Paola and Seal (1995) addressed the seeming contradiction between the concept of equal mobility for sediment entrainment and systematic downstream fining by showing mathematically that equal mobility can in fact produce downstream fining when the bed texture is considered as a mosaic of heterogeneous ‘patches’ instead of a spatially homogeneous grain-size mixture. They argued that equal mobility can be satisfied within each patch, and that coarser patches with larger median grain-sizes are transported at lower rates than finer patches. In an accompanying empirical study, they confirmed that this model sufficiently accounts for field observations of downstream fining on the North Fork Toutle River (Seal and Paola, 1995). This advance to our understanding of fluvial process was facilitated by observations of the systematic pattern of downstream fining, which illustrates the utility of empirical datasets in driving forward fluvial theory by forcing physical explanations to reproduce the patterns observed in actual rivers.

Given the traditional limitation in collecting high resolution grain-size measurements across vast spatial extents, it is worth questioning whether systematic

grain-size sorting patterns within river systems have gone unnoticed. Advancements to fluvial remote sensing techniques have allowed researchers to capture high resolution information at larger areas (e.g. Fonstad and Marcus, 2010; Dietrich, 2016; Zettler-Mann and Fonstad, 2020). These surveying developments enable data-driven approaches for researching fluvial form and process (Fonstad and Zettler-Mann, 2020), which may uncover systematic patterns – or geomorphic signals – that can inform theories of physical processes such as sediment transport and channel development.

Multiscale observations of river environments allow researchers to engage with the complexity within river environments, rather than smoothing over local heterogeneity in favor of capturing larger extents or conducting intensive analyses at local scales. This presents another application of fluvial remote sensing: novel evaluations of our conceptual frameworks for relating geomorphic information across scales such as downstream hydraulic geometry, the river continuum concept, sediment links, and the process domains concept. Fonstad and Marcus (2010) introduced the importance of multiscale data for identifying patterns and comparing fluvial models. Zettler-Mann and Fonstad (2020) leveraged this approach to evaluate the utility of the sediment links concept for explaining downstream patterns on the Rogue River. Their work shows that our geomorphic questions and theories reflect our observational techniques, and recent advancements to surveying methods present a continued opportunity to advance our understanding of river form and process (Fonstad and Zettler-Mann, 2020).

In this article, I focus specifically on mapping coarse sediment grain-size variability within gravel bars and across a 12 km river segment. Although admittedly limited in the representation of components of a river system, measuring patterns in grain-sizes is commonly employed to characterize important fluvial patterns and processes such as local versus upstream controls on sediment supply, salmonid habitat, and downstream fining rates. Fonstad and Zettler-Mann (2020) raise questions about the implications of our particle size sampling techniques, such as identifying beforehand the sample spacing necessary to capture the patterns of sediment sorting that are important for understanding processes of interest including habitat suitability and channel development. Below, I apply a set of methods capable of capturing high resolution and

precision grain-size data across a large extent of the upper Sandy River and leverage the resulting dataset to analyze grain-size variability at river segment and gravel bar scales and suggest potential morphological sources of the observed variability.

2. Methods: Grain-Size Map Production

The desired dataset consists of observations of patch scale coarse sediment grain-size distributions across gravel bars within a 12 km reach of the upper Sandy River. The term ‘patch’ is used in this study to describe the spatial extent of individual samples similar to Chardon et al. (2020), rather than its traditional use as a synonym for grain-size facies in reference to discrete zones on the bed surface of varying area that are distinguished by researchers based on a characteristic grain-size (e.g. Buffington and Montgomery, 1999). Along with grain-size percentiles, each observation should include multi-scale geographic attributes that convey the sample’s location within a gravel bar and the river system, as well as geomorphic metrics such as channel width and slope. The methods for producing such a dataset are dependent on a remote sensing approach using images to locate samples and estimate grain-sizes. Previous work (Chapter 2) investigating the suitability of image-based grain-size surveying and measurement techniques for creating such a multi-scale grain-size map of coarse sediment suggested combining drone-based images, directly georeferenced structure from motion (SfM) to obtain accurate image locations and resolutions, and the PebbleCounts photosieving software for estimating grain-sizes from the non-orthorectified images. This section describes the application of this approach to the upper Sandy and introduces a few efficient methods for characterizing each grain-size sample’s basic morphological setting.

2.1. Study Area

The upper Sandy River (Figure 11) drains the flanks of Mt. Hood in northern Oregon, USA and is characterized by its steep valley, large floods, and abundant sediment. The natural river dynamics are defined by its geomorphic history including glacier activity that carved the valley from volcanic bedrock, and volcanic emissions from Mt. Hood that have deposited masses of ash and rock fragments into the valley bottom (Cameron and Pringle, 1986; Handelman et al., 2014). The Timberline Lahar

1,700 years ago and the Old Maid Lahar 200 years ago introduced incredible volumes of sediment ranging from sand to boulders, forcing the Sandy River to readjust its form through incision, lateral migration, channel widening, and avulsions. These adjustments have organized sediment into gravel bars, which continue to develop during high flows today. The growth and erosion of these bars play a central role in driving channel adjustments and sediment transport rates (Handelman et al., 2014).

The adjustments described above are punctuated rather than continuous – usually driven by flood events. High magnitude flows interact with the sediment within the channel as well as the unconsolidated and easily erodible lahar deposits that form much of the river bank. A 250-year flood occurred in 1964 that devastated nearby communities as it destroyed roads, bridges, and entire neighborhoods. More recently, a 40-year flood in 2011 caused significant damage to infrastructure along the upper Sandy. These events have caused nearby communities to seek an understanding of the natural river dynamics and its relation to channel migration hazards and salmonid habitat. Ongoing restoration efforts organized by the Sandy River Watershed Council focus on buffering development from the river channel to provide room for channel migration and avulsions and reconnecting floodplains and side channels to improve habitat while dissipating the river's energy (Handelman et al., 2014).

The downstream boundary of the study site drains 318.6 km² of forested (87% forest cover) and steep terrain. The average channel slope within the 12 km study segment is 0.013 m/m and the average active channel width is 40 m. The area receives a mean annual precipitation of 97.4 with additional streamflow generated from glacier melt on Mt. Hood during the warm season. Elevation above sea level ranges from approximately 460 m at the upstream boundary of the study site to 300 m. The watershed contains very little human development, however the infrastructure and developed properties that do exist are in relatively close proximity to the river corridor.

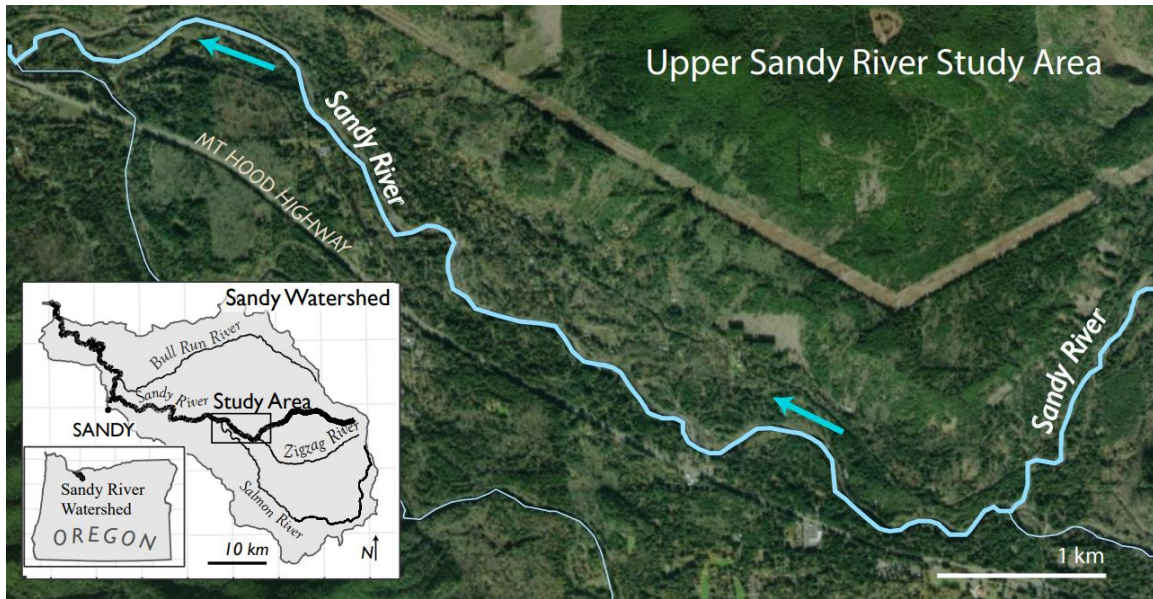


Figure 11: A map of the study site on the Upper Sandy River, Oregon, USA.

2.2. Image Acquisition

Fieldwork was conducted during multiple trips to the upper Sandy River between August 15, 2020 and September 10, 2020. Figure 12 shows the hydrograph approximately 20 km downstream of the study site for the 2020 water year. The field season is marked by the red box, which indicates that images were collected during the lowest flows of the year and with the greatest area on gravel bars exposed.

Drone-based surveys were conducted for individual gravel bars following the protocol presented by (Carbonneau and Dietrich, 2017) for directly georeferenced (DG) SfM photogrammetric surveys. I followed a protocol by Carbonneau et al. (2018) to extend this DG workflow to include non-overlapping near ground images designated for photosieving. SfM processing was used to calibrate the altitude above ground level (AGL) and image scale for these individual images within the photogrammetric block. This DG workflow enabled efficient field surveys by predicting the scale of individual images within 3% and survey sites (e.g. gravel bars) within 1% without any calibration in the field (Carbonneau et al., 2018).

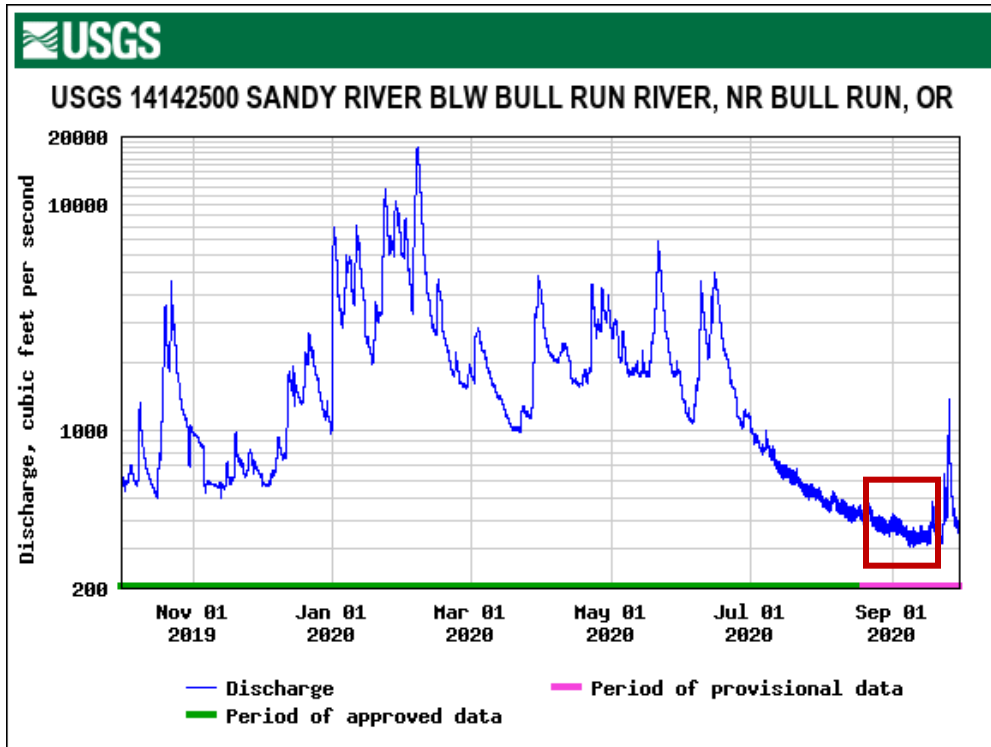


Figure 12: Hydrograph for Water Year 2020 at the USGS operated gage downstream of the study site. The time span for fieldwork is marked by the red box.

Previous work on SfM for geomorphic mapping shows that multiple camera heights and convergent imagery can mitigate systematic error in mapping products (Fonstad et al., 2013). For each gravel bar survey, nadir imagery was collected from 18 m AGL using automated flight plans and image intervals in the Litchi application specifically designed to produce 80% forward overlap and 50% sidelaps. Images were also acquired from 60 m AGL at 30 degrees off-nadir using manual flight operations in order to avoid collisions with the tall vegetation canopy within the study site. These 60 m AGL images were positioned to converge on the study site and overlap with the 18 m nadir images. In addition to these higher altitude photos, near-ground images at 3 m AGL were acquired to provide millimeter scale high-resolution images suitable for delineating grains in the photosieving process. The near-ground images were non-overlapping for more efficient surveying.

2.3. Obtaining Image Location and Resolution

Multiple gravel bars were surveyed on each day of fieldwork, so a data

management strategy was required to ensure that the correct images were grouped into SfM projects. Each gravel bar was assigned a unique name (e.g. ‘A’, ‘B’, ‘C’, etc.), which was used to organize image processing. Timestamps were recorded in the field upon the beginning and end of the survey of each gravel bar. In the evening, these timestamps were used to sort images into unique folders for each gravel bar and rename image files. For example, an image taken of Bar ‘C’ named ‘DJI_0001’ was renamed to ‘C_DJI_0001.’ Due to the large number of files, the image renaming process was automated.

2.3.1. Structure from Motion Processing

Each gravel bar was processed as an independent project in Agisoft Metashape using the collection of the 60 m, 18 m, and 3 m images. The objective of SfM processing was to produce the necessary ingredients for calculating an accurate image scale for the non-orthorectified near ground images: an orthophoto, a DEM, and the aligned camera locations for all images. A standard SfM processing workflow described by Carbonneau et al. (2018) was used for each project to align cameras and build dense clouds, orthomosaics, and DEMs. The orthophotos and DEMs were exported as GeoTIFFs from Agisoft Metashape and imported into ArcGIS Pro. Camera locations for all images (3m, 18 m, 60 m) were exported as Extensible Markup Language (xml) files into a common folder. A Python script was written to parse each of these xml files and concatenate every individual’s unique label, latitude, longitude, and elevation into a single camera location data matrix.

2.3.2. Image-scale calculation

Converting the photosieved grain-size measurements in pixels to metric units requires accurate image scales in mm per pixel. The camera specifications such as field of view, focal length, and image size were known entities, however the camera’s altitude AGL at the time of image acquisition must be calculated using the camera locations and DEMs exported from Agisoft Metashape. Every DEM raster pixel value that corresponds with a camera location was sampled and attached to that camera’s label using the ‘Extract Values to Points’ tool in ArcGIS Pro. A Python script automated the task of matching bar

elevations to the corresponding image in the matrix of camera location information. This script also calculated the camera's altitude AGL by subtracting the bar elevation from the camera elevation for each image. The image resolution was also calculated using the camera specifications and the altitude AGL. Lastly the script copied all image files with an altitude AGL less than 4 m from the original individual bar folders to a new folder consisting of only the high-resolution images designated for photosieving.

2.4. Grain-Size Attributes

Photosieving in PebbleCounts requires commandline arguments to designate image file locations and resolution among other settings described by Purinton and Brookhagen (2019). Given PebbleCounts' significant processing time of 5-10 minutes per image, I automated the production of the commandline arguments for each image for the sake of efficiency. A new Python script looped through every high-resolution image to write its unique commandline argument that can easily be pasted into the terminal. PebbleCounts was run in accordance with the accompanying manual available for download at the PebbleCounts Github. Photosieving in PebbleCounts produces a matrix for each image (i.e. sample) in which rows represent individual grains and columns provide measurements such as a and b axes measured in both pixels and meters. The only alteration to the algorithm was a change to the output file location, so the matrices of grain-size measurements stored in csv files were all written to the same folder and named using each image's unique label.

Comparisons among each of the 463 samples depend upon a common description of the grain-size distribution that can be stored in a single matrix. A newly developed automated tool looped through each PebbleCounts output matrix to remove any grains smaller than 16 mm and calculate the following percentiles: D_5 , D_{10} , D_{16} , D_{25} , D_{50} , D_{75} , D_{84} , D_{90} , D_{95} . These percentiles were calculated in both *millimeters* and *psi* ($psi = -phi = \log_2 mm$). The script also merged each sample's unique label and percentiles into a single row within a master grain-size matrix.

2.5. Geographic Attributes

Although each sample covers an area of approximately one square meter, their

geographic locations are represented as points based on the latitude and longitude recorded by the drone GPS upon image acquisition and corrected during SfM processing. Representing each sample’s location involves leveraging the latitude and longitude coordinates exported from Agisoft Metashape to obtain samples’ river-scale and bar-scale coordinates. I automated a process to parse the latitude and longitude coordinates from their individual xml files and merge these coordinates into a single csv file, which I subsequently projected to a UTM coordinate system. The remainder of the geographic transformations utilized these UTM coordinates. Table 1 shows the geographic attributes attached to each sample and the process for producing those attributes are described below.

Table 4: Geographic attributes attached to each grain-size sample and its associated spatial scale.

Attribute	Abbreviation	Scale
Latitude	Lat	Global
Longitude	Lon	Global
X (UTM)	X	Global
Y (UTM)	Y	Global
Distance Downstream	Ds	River
Cross Stream	Xs	River
Bar Name	Bar	Bar
Distance Downbar	Db_dist	Bar
Normalized Distance Downbar	Db_norm	Bar
Distance from Bar Edge	Edge_dist	Bar

2.5.1. River Scale Locational Attributes: Channel-fitted Coordinate System

The channel-fitted coordinate system presented by Legleiter and Kyriakidis (2006) and described in Chapter 2 represents points based on their streamwise (s) and stream-normal (n) positions relative to a defined channel centerline. The transformation from UTM (x, y) locations to channel-fitted (s, n) coordinates requires a csv file containing the UTM coordinates of regularly spaced points along the centerline. To

produce this file, the channel centerline was manually digitized in ArcGIS Pro based on National Aerial Imagery Program (NAIP) imagery acquired in July 2020 at a consistent scale of 1:2,000. Decisions for defining the channel centerline were not significant factors in this study as changes in the centerline's path through time are not part of the analysis. Nevertheless, I defined the centerline based on the dominant low flow channel, determined by channel width and experience floating the channel during fieldwork. Figure 13 shows the digitized centerline over the 2020 NAIP imagery across a reach with multiple low flow channels. The UTM (x, y) coordinates for points spaced every 1 m along the digitized centerline were exported from ArcGIS Pro as a csv file. This file and a matrix of grain-size sample labels with their UTM (x, y) coordinates comprised the two inputs to a Python script (Dietrich, 2019) to automate this transformation using the default transformation parameters aside from setting $rMax$ to 50, which is the maximum perpendicular distance in meters from the centerline that the code will search for points.

The output of the coordinate transformation was a matrix in which each row represented an individual grain size sample with the following attributes: *label, x, y, s, n*. The (s, n) coordinates provide a simple representation of the location of each patch sampled within the river system. The s coordinate reveals the *downstream distance* from the study area's upstream boundary to a given sample, while the n coordinate provides the sample's *cross stream* distance from the digitized centerline.

2.5.2. Bar Scale Locational Attributes

All samples included in the study are associated with one of 33 gravel bars. A sample's location within this bar is described by its distance down bar and its distance from the bar edge. I used methods analogous to calculating samples' *downstream distance* to identify the *downbar distance* by replacing the channel centerline with a digitized bar centerline in the channel-fitted transformation. I processed each gravel bar separately using its unique centerline and the associated samples' (x, y) coordinates. The output of these transformations provides the sample's *downbar distance*. In order to make comparisons among gravel bars of varying size, the *downbar distance* attribute was used to calculate *downbar normalized* using Equation 1 where d_n is *downbar normalized*, d_b is

downbar distance, and b is the bar's total length measured from head to tail:

$$(1) \quad d_n = \frac{d_b}{b}$$

Bar edge distance was measured using a digitized boundary between each bar's exposed surface and the water's edge. I developed an automated tool to measure the minimum Euclidean distance between every within a bar sample and the digitized boundary. I attached these bar-scale attributes to the master data matrix based on the unique label for each grain-size sample to produce associations between grain-size percentiles and bar and river-scale geographic attributes.

2.6. Morphological Attributes

I extended the dataset to provide basic information regarding the morphologic setting using commonly available datasets such as aerial imagery and large-scale topography. Below, the local active channel width and reach-scale water surface slope are quantified and attached to each grain-size sample. These attributes were chosen based on their physical connection to grain size, data availability, and potential for automating their measurement for each sample.

2.6.1. Active Channel Width

Active channel width quantifies the area that is undergoing fairly regular bed reworking (i.e. sediment transport) by measuring the width of the unvegetated floodplain perpendicular to the channel centerline (see Figure 13). The assumption underlying this measurement is that the influence of bed reworking prevents riparian vegetation from colonizing these areas, and vegetated portions of the floodplain are included in the active channel in areas where they separate active channels (East et al., 2017; O'Connor et al., 2003). The active channel widths were manually measured at 70 m intervals (roughly two channel widths) along the channel centerline using 2020 NAIP imagery. Figure 13 provides a visual key for the determination of active flow zones.



Figure 13: Examples of centerline (blue) and transects (orange) measuring the active channel width in multi-threaded reaches.

The *active channel width* for a given grain-size sample was calculated using the two nearest transects as shown in Figure 14. The equation within the image calculates the weighted average of the upstream and downstream channel width measurements. The weights are based on the sample's distance from each transect. To automate this calculation, the (x, y) locations for each transect's intersection with the channel centerline were first transformed to the channel-fitted coordinate system. A new Python script automated the *active channel width* calculation using the master grain-size matrix as well as the transect downstream locations and widths. The script also attached the resulting width as a column in the master matrix.

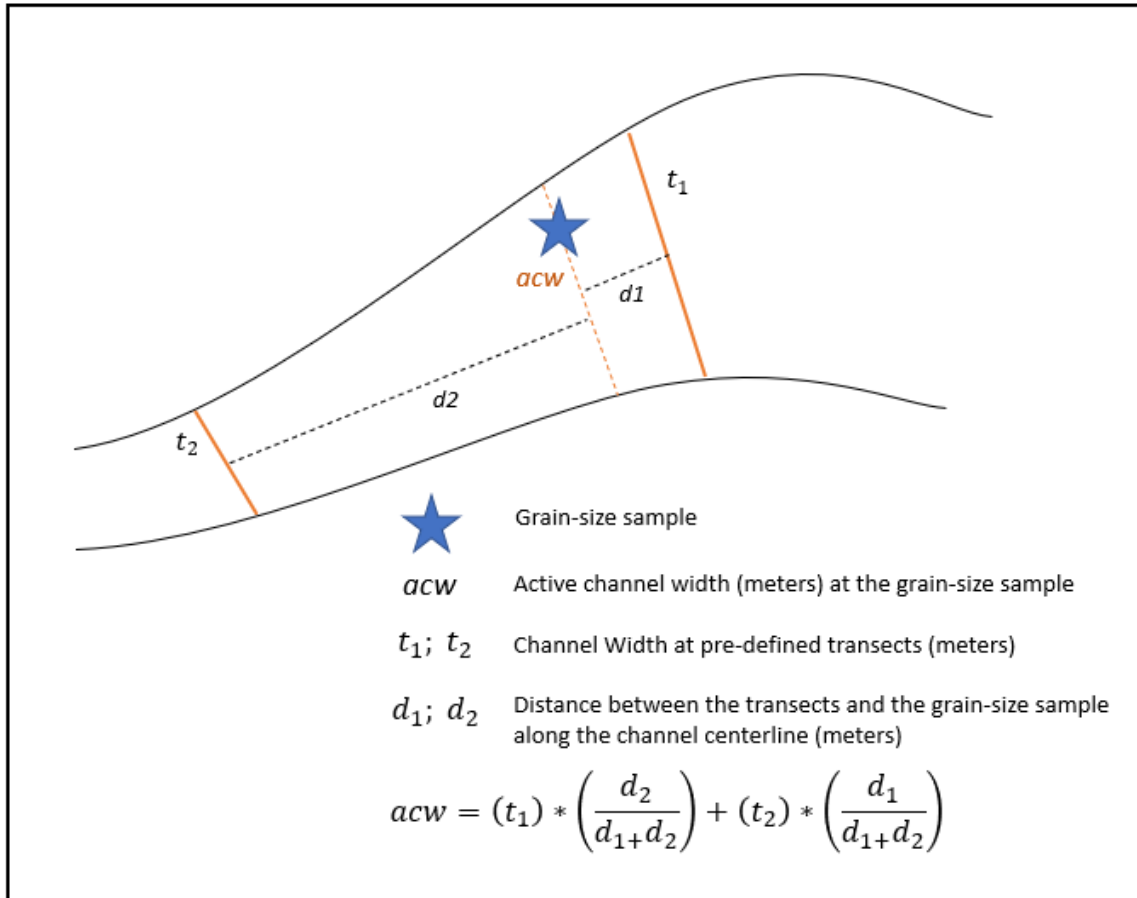


Figure 14: Diagram of the method for interpolating the active channel widths for each grain-size sample from the transect measurements.

2.6.2. Slope

A longitudinal profile is a prerequisite for attaching the *slope* attribute for each grain-size sample. A LiDAR-derived DEM available through Oregon’s Department of Geology and Mineral Industries (DOGAMI) provided the topographic information to produce the longitudinal profile. The LiDAR survey took place in 2011 shortly after a 40-year flood event, which gave rise to the most recent major reconfiguration of channel morphology on the upper Sandy River. The longitudinal profile in this study used the water surface elevation due to the near-infrared (NIR) LiDAR survey, which is not capable of accurately measuring channel bathymetry on the Upper Sandy. The primary concern in using the 2020 centerline was the possibility that changes to the river channel over the preceding nine years could cause the digitized path to lie outside of the channel in the

2011 DEM. In this case the longitudinal profile would reflect bank and floodplain topography rather than the water surface. In order to determine whether the use of a 2011 topographic survey was appropriate for relating water surface slopes to the 2020 grain size samples, I produced and compared two longitudinal profiles. The first profile was derived solely from the 2011 LiDAR survey using the procedure described by Cavalli et al. (2008):

1. Remove local depressions using the 'Fill' tool in ArcGIS Pro.
2. Determine flow directions using the D8 algorithm within the Flow Direction tool in ArcGIS Pro.
3. Calculate the number of contributing cells using the 'Flow Accumulation' tool in ArcGIS Pro, and then reclassify the output raster using a constant threshold to distinguish the stream network.
4. Convert the stream cells tool to a polyline using the 'Stream to Feature' tool.
5. Generate points spaced every 1 m along the stream polyline and use their elevation on the DEM to produce the longitudinal profile.

The second longitudinal profile was produced using the same DEM and the low flow centerline digitized based on the 2020 NAIP imagery. Figure 15 shows a comparison of the DEM-derived path and the NAIP-derived path. I visually inspected these two paths with the 2011 DEM and hillshade layers at a scale of 1:1200 (Figure 15) across the entire study area in search of locations where the 2020 centerline deviates from the 2011 channel water surface. With no significant deviations, I moved forward using the 2020 centerline to produce the longitudinal profile (Figure 16) for the purpose of compatibility with the downstream distances associated with each grain-size sample.

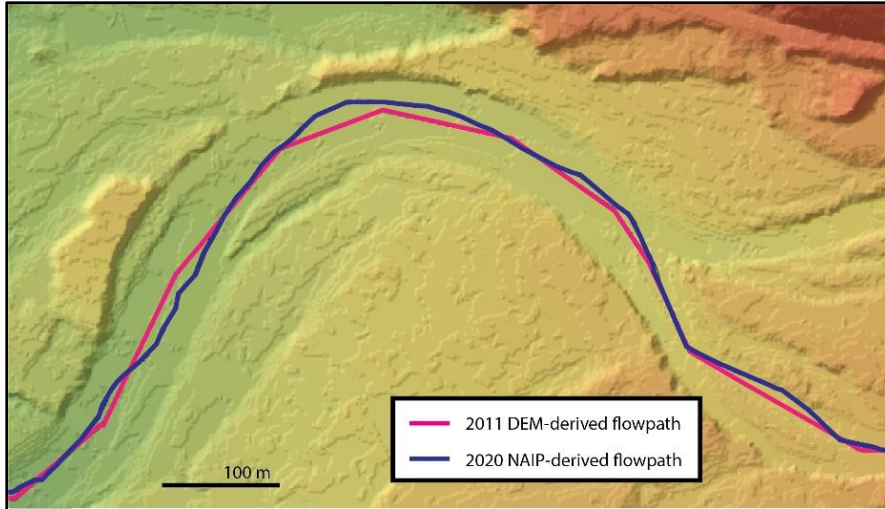


Figure 15: Comparison of the channel centerline derived from the 2011 LiDAR survey and from manually digitizing the dominant low-flow channel from 2020 NAIP imagery.

I transformed the (x, y, z) coordinates for evenly spaced points along the channel centerline to the channel-fitted coordinate system to produce (s, n, z) points. The resulting s -coordinates represent the distance downstream, the n -coordinates are all equal to zero, and the z -coordinates remain unchanged. The longitudinal profile shown in Figure 16 is a plot of the z (elevation) vs. s (streamwise) coordinates.

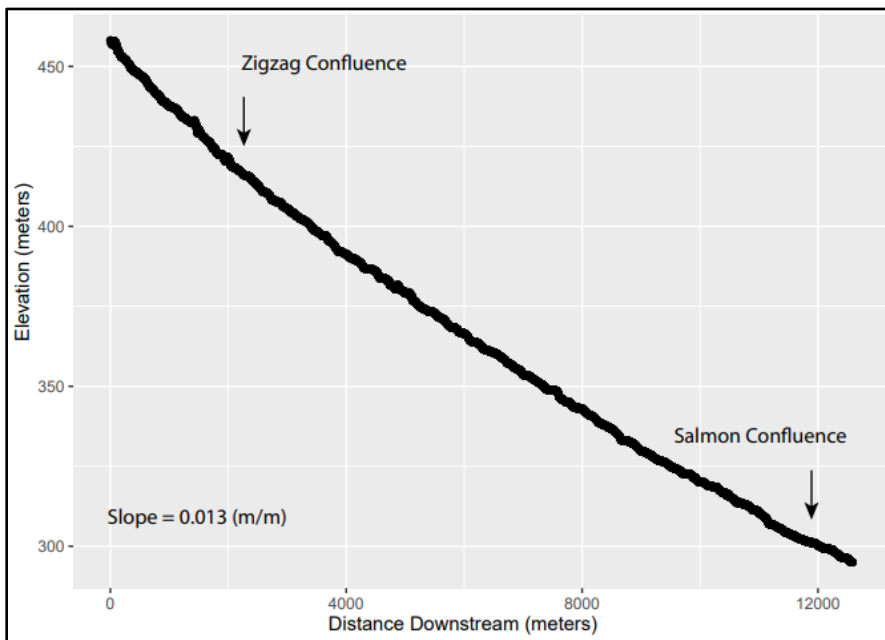


Figure 16: Longitudinal profile of the study site.

The use of water surface elevations for developing a one-dimensional longitudinal profile as well as the likelihood of morphologic adjustments during the nine-year span between the topographic and grain-size surveys prevent the characterization of local slopes in the immediate area surrounding each grain-size sample. Instead, *slopes* were calculated using points on the channel centerline located 50 m upstream and downstream from each sample. Again, I automated this calculation and attached the results to each sample in the master grain-size matrix.

2.7. Multi-Scale Grain-Size Map

This grain-size mapping effort produced a dataset of 463 observations of patch-scale grain-size distributions associated with geographic topological attributes and channel morphology metrics. Table 5 provides a description of the grain-size, geographic, and morphological attributes attached to each sample. The distribution of the samples within the study area is displayed in Figure 17, along with examples of the available grain-size information available at the bar and patch scales.

Table 5: Attribute descriptions for each grain-size sample within the dataset.

Attribute	Description
Label	Unique to each sample based on bar name and original image file.
Grain-Size Percentiles (mm)	D ₅ , D ₁₀ , D ₁₆ , D ₂₅ , D ₅₀ , D ₇₅ , D ₈₄ , D ₉₀ , D ₉₅ calculated from PebbleCounts outputs with a 16 mm lower truncation
Grain-Size Percentiles (psi)	D ₅ , D ₁₀ , D ₁₆ , D ₂₅ , D ₅₀ , D ₇₅ , D ₈₄ , D ₉₀ , D ₉₅ calculated from PebbleCounts outputs with a 4 psi lower truncation
Latitude	GPS coordinates exported from Agisoft Metashape
Longitude	GPS coordinates exported from Agisoft Metashape
X	Location coordinates projected to the UTM coordinate system
Y	Location coordinates projected to the UTM coordinate system
Bar	Delineates the bar from which the sample was obtained
Distance Downstream (m)	Distance in meters downstream along the channel centerline from the upstream boundary of the study area
Cross Stream (m)	Distance from the channel centerline
Distance Downbar (m)	Distance in the downstream direction from the bar head
Distance from Edge (m)	Shortest distance from the bar edge
Active Channel Width (m)	Width of the active flow zone interpreted from aerial imagery
Slope	Water surface slope of the 200 m surrounding the sample
Bar Type	Classified bar morphology based on Charlton (2007).

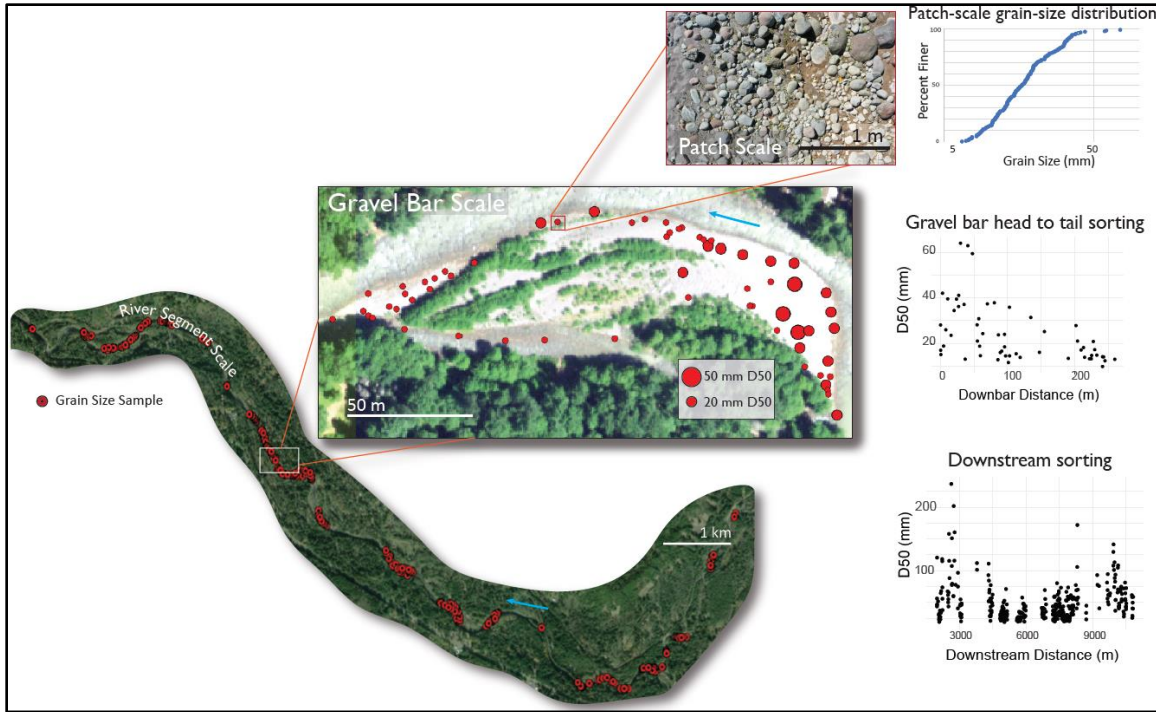


Figure 17: Multiscale grain-size information mapped in the upper Sandy River

3. Grain-Size Sorting

The dataset above enables quantitative descriptions of sediment sorting and its relation to channel morphology throughout the study area. Two general statistical approaches are employed to describe the sources of grain-size variability. The first is to compare the distribution of grain-sizes among different groups of samples based on geographic and morphological attributes such as bar membership and bar-scale position. The underlying objective of these statistical analyses, such as analysis of variance (ANOVA) and Bartlett’s test, is to determine whether our knowledge of a given attribute should influence our expectation of that sample’s grain-size. The second category of statistical approaches includes various regression analyses, which follow the conceptual model that *grain-size = predictable component + noise*, in which the predictable component is derived from geographic and morphological information about the samples, such as streamwise position or active channel width. The significance of the relationship between grain-size and the predictor variable of interest can be described by regression outputs that reflect the ratio of signal (i.e. predictability) vs. noise in grain-size response.

My analysis uses the psi grain-size scale instead of millimeters due to the long-tailed distribution of metric b -axis lengths (Figure 18). The conversion from mm to psi ($\psi = \log_2 mm$) is important because many of the statistical techniques used here assume that the response values are normally-distributed.

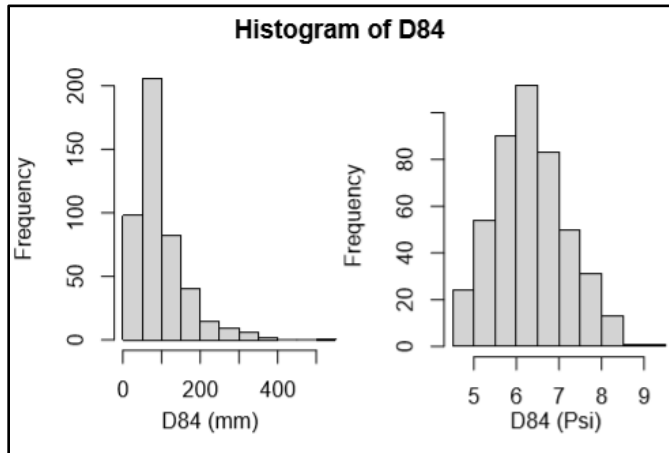


Figure 18: Comparison of D_{84} histograms for grain-sizes measured in millimeters (left) and psi (right).

3.1. Downstream Grain-Size Variability

Downstream sediment sorting patterns can be evaluated through grain-size response to downstream distance. It is important to note that specific regression techniques analyze different aspects of the relationship between grain-size and downstream distance. For example, the following hypotheses make different statements regarding downstream grain-size sorting:

H1: Grain-sizes will decrease in the downstream direction.

H2: Grain-sizes are autocorrelated with upstream observations of grain-size.

H1 refers to a *global* relationship among grain-size and streamwise position, while H2 seeks an understanding of *local* relationships throughout the study area. A global statistical analysis, such as OLS linear regression, defines a relationship by drawing a curve that is optimized while considering the entire dataset. This approach lends itself to understanding patterns such as downstream fining, and therefore the significance of the relationship produced by a linear regression between grain-size and downstream distance is used to test H1.

Nonparametric regression takes an alternate approach by re-calculating the local relationships between response and predictor variables with a moving window throughout the dataset, which is most commonly seen through scatter-diagram smoothing. The relationship produced by nonparametric regression is formed without initial assumptions of the overall form of the relationship and the resulting ratio of signal from the smoothing component and noise reflects how similar nearby observations are relative to the entire population. Put differently, a smoothing curve drawn through a scatter plot of grain-size vs. downstream distance that does not offer a significant predictable component for grain-size indicates that nearby grain-sizes are randomly distributed across the streamwise axis.

The OLS regression among median grain-size and downstream distance employed to test H1 produced a slight yet statistically significant decrease in grain-size in the downstream direction. The slope indicates a median *b*-axis reduction of 0.2 mm/kilometer within the study site. Despite the statistical significance, we should be wary of claiming that grain-size varies systematically with downstream position given the degree of precision of the photosieving methodology. Median grain-size is plotted against downstream position in Figure 19 with a red line representing the OLS regression.

The general additive model (GAM) utilized to test H2 is analogous to the blue smoothing curve displayed in Figure 19. The GAM produced a p-value less than $2.2e-16$, suggesting that median grain-size is significantly related to nearby samples. Although the GAM shows that grain-sizes vary with streamwise position, it fails to characterize the spatial scale at which patch-scale median *b*-axis length is related. Autocorrelation is oftentimes applied to time-series to investigate a variable's association with its previous value. This approach has been extended to spatial autocorrelation to investigate how a variable is correlated with nearby observations while accounting for multiple spatial dimensions (i.e. *x*, *y*, *z*). Time-series autocorrelation methods turn out to be very applicable to H2 given the single streamwise dimension. Therefore, I tested the correlation of median grain-size with itself at various downstream lags (Figure 20). The results indicate that grain-size is serially correlated along the streamwise axis, but this effect degrades within 50 m.

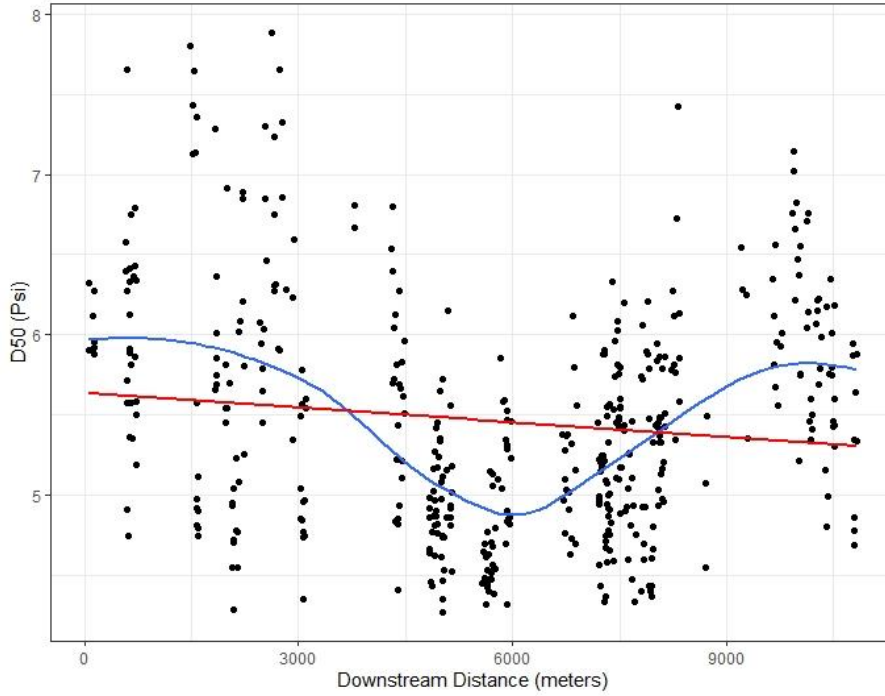


Figure 19: Median grain-size vs. downstream position. The red line visualizes the statistical approach of an OLS regression, and the blue curve reflects the general approach of the general additive model used to test H2.

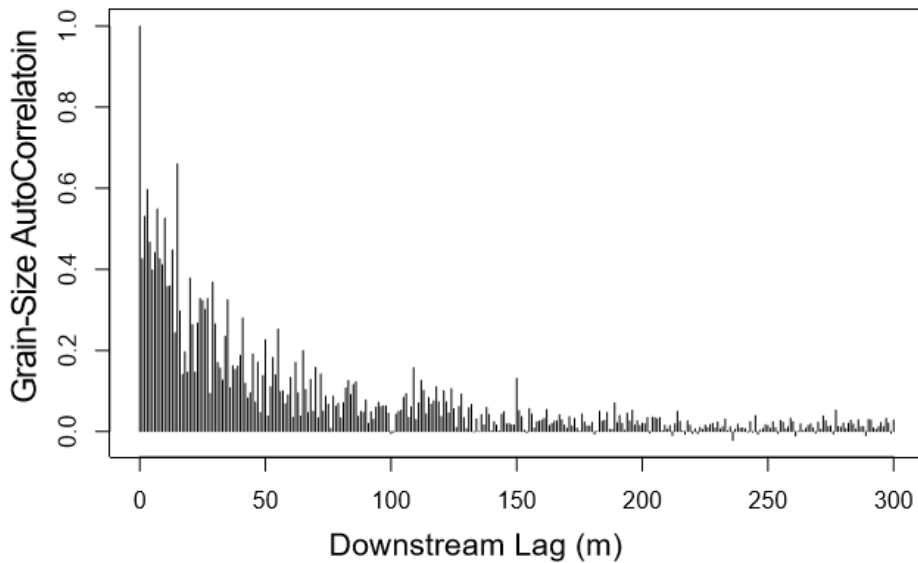


Figure 20: Correlogram of median grain-size at various downstream lags computed using a time-series autocorrelation.

3.2. Bar-scale Sorting

The grain-size samples can be classified into groups based on bar membership and position within the bar head or bar tail, which enables statistical evaluations of the differences among these groups. Grain-size response to bar-scale location is evaluated across the entire dataset and within individual bars to address the following hypothesis:

H3: Sediment grains are larger at bar heads compared to bar tails.

The global relationship between D_{50} and downbar position is presented in Figure 21 based on metric distance from the barhead (A), downbar distance normalized by the size of the bar (B), and through a comparison of the distribution of median grain-size classified by bar head and bar tail (C). The means are not significantly different based on an analysis of variance (F-Statistic = 0.468; P-Value = 0.494), however a Bartlett's test shows that the variance of bar head median grain-size is significantly larger than bar tails ($K^2 = 24.397$; P-value = $7.838e-07$). Although the median bar head D_{50} is smaller than the median bar tail D_{50} , visual inspection of Figure 21 A and B suggests that the coarsest grains within the river system are positioned at bar heads and that these coarsest samples decrease downbar.

The validity of H3 was also evaluated on the basis of individual bars (Table 6). These results suggest significant variability in bar scale sorting among the 33 gravel bars. ANOVAs testing the differences among bar head and bar tail mean grain-sizes for each bar showed that 8 bars had significantly different head to tail grain-sizes. Bartlett tests examining differences in the variance of each group showed that 5 gravel bars had significantly different head to tail grain-size variance.

Comparisons of grain-size variability within and among gravel bars (Figure 22) shows that the range of patch-scale median grain-sizes within some gravel bars are nearly equivalent to that observed within the entire study area. This result demonstrates the importance of local and bar scale sediment sorting processes within the upper Sandy River. It also likely reflects the distinct sediment supply regime that introduces a wide

range of sediment sizes into the river system.

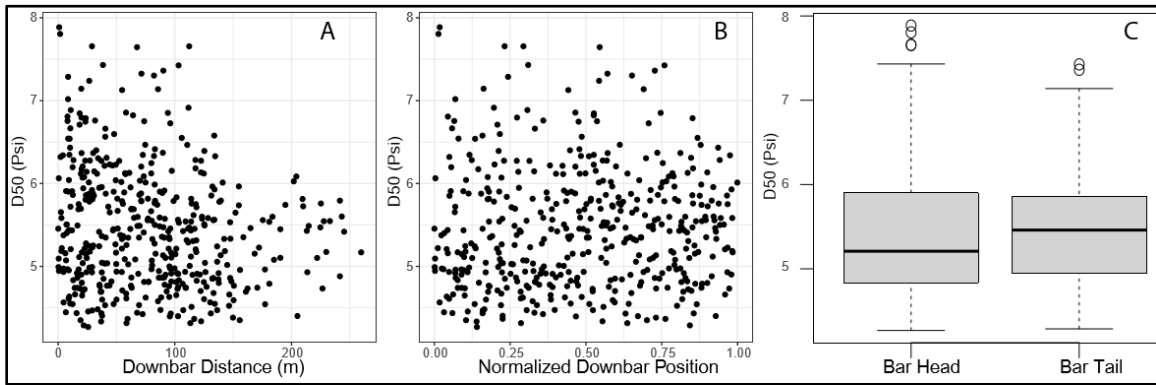


Figure 21: Median grain-size vs. downstream distance from the barhead (A); Median grain-size vs. downbar position normalized by gravel bar length (B); and boxplots comparing the D_{50} of patches located within bar heads and bar tails (C).

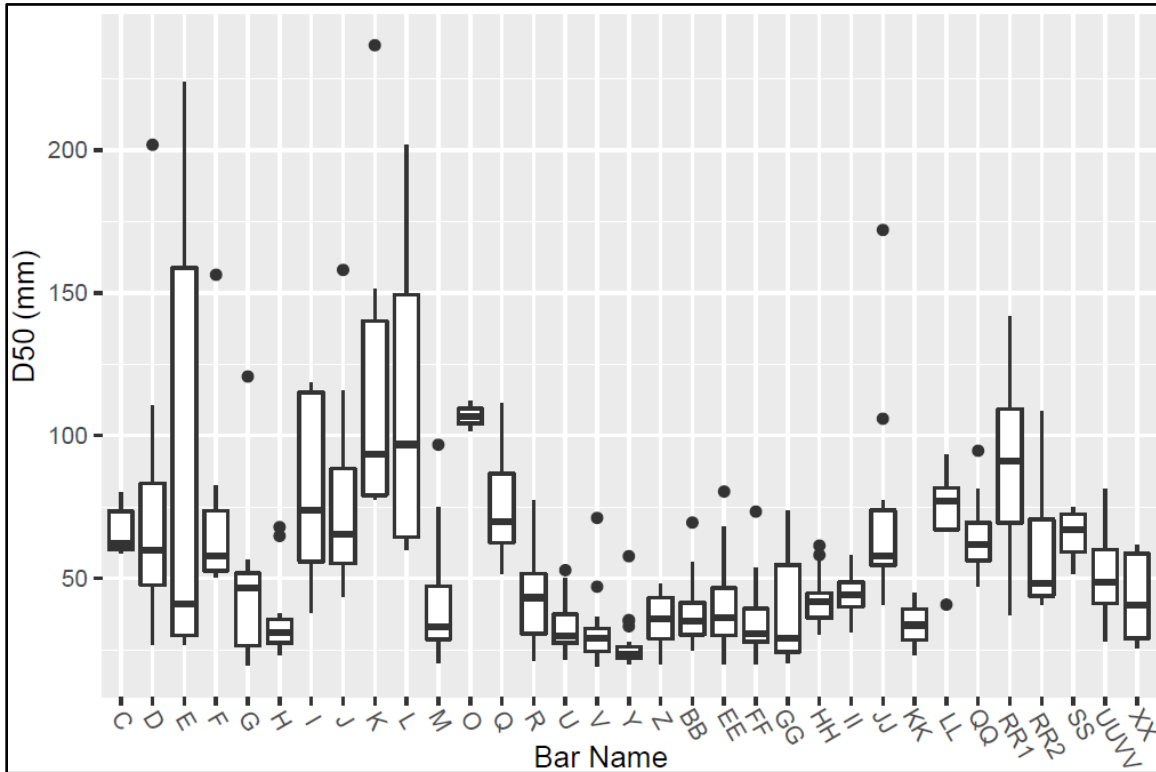


Figure 22: Variability in patch scale median grain-size among gravel bars within the study area.

Table 6: Statistical descriptions of the differences in median grain-size with bar heads and bar tails for each individual gravel bar within the site. Four gravel bars did not have enough observations at the bar head or tail to conduct an ANOVA or Bartlett's test. Significant results are shown in bold. The fining rate is dimensionless and represents the inverse of the coefficient to multiply bar head grain-sizes to calculate bar tail grain-sizes. Positive fining rates indicate downbar fining and negative values indicate downbar coarsening.

Bar	Downstream Distance (m)	Active Width (m)	ANOVA F-Statistic	ANOVA P-value	Bartlett K ²	Bartlett P-value	Bar head D ₅₀ (mm)	Bar tail D ₅₀ (mm)	Fining Rate
C	66.09232	28.81838	0.711	0.488	2.5479	0.1104	69.89159	61.38765	0.121673
D	577.5483	36.62233	0.149	0.705	3.7324	0.05337	64.97442	69.54361	-0.07032
E	1476.522	37.39758	13.32	0.00446	0.13992	0.7084	198.1569	30.84887	0.844321
F	1832.037	15.18182	0.63	0.511	2.7387	0.09794	103.3393	61.2274	0.407511
G	1983.204	48.38453	3.931	0.0947	5.1298	0.02352	46.61987	26.09659	0.440226
H	2068.053	52.63428	4.123	0.098	3.8181	0.0507	30.97705	50.95053	-0.64478
I	2216.842	28.8779	NA	NA	NA	NA	118.3623	38.11354	0.677993
J	2466.575	32.76882	7.231	0.115	1.1908	0.2752	64.66913	101.9966	-0.57721
K	2629.772	27.83181	322218	0.00112	1.1908	0.2752	79.25139	236.6353	-1.98588
L	2720.813	26.5404	0.097	0.785	1.1908	0.2752	60.08445	77.91999	-0.29684
M	2925.528	59.36405	12.75	0.00602	3.6607	0.05571	75.07654	29.15316	0.611687
O	3785.176	57.54698	NA	NA	NA	NA	NA	NA	NA
Q	4302.301	50.18533	0.915	0.393	5.9656	0.01459	93.07365	69.79232	0.250139
R	4362.095	48.25068	1.496	0.249	0.96104	0.3269	30.63673	49.12401	-0.60344
U	4832.218	101.6055	8.177	0.0126	4.7776	0.02883	28.15737	37.34541	-0.32631
V	5000.303	116.5441	5.413	0.0335	1.2165	0.2701	25.53513	30.38834	-0.19006
Y	5581.129	88.57917	0	0.988	1.0616	0.3029	23.41744	25.50088	-0.08897
Z	5795.735	48.01631	0	0.995	2.1968	0.1383	33.51442	29.05291	0.133122
BB	6704.195	48.96098	0.92	0.36	3.0606	0.08021	36.54966	41.36491	-0.13175
EE	7204.153	74.78024	10.95	0.00187	0.03448	0.8527	34.71881	44.63558	-0.28563
FF	7562.82	65.26251	0.125	0.73	0.11638	0.733	35.63752	30.48148	0.14468
GG	7816.939	32.11673	5.393	0.0453	4.0037	0.0454	41.59098	24.34392	0.414683
HH	8009.067	41.33461	1.53	0.247	0.35225	0.5528	43.29632	36.41578	0.158917
II	8123.319	26.58445	NA	NA	NA	NA	31.13431	58.19533	-0.86917
JJ	8231.454	31.11721	0.415	0.548	0.98145	0.3218	66.21334	70.26004	-0.06112
KK	8707.817	22.88421	NA	NA	NA	NA	33.65978	45.05315	-0.33849
LL	9205.764	18.18441	2.012	0.292	0.4113	0.5213	85.56115	58.39336	0.317525
QQ	9649.259	19.11581	1.124	0.349	0.87284	0.3502	68.87536	61.46793	0.107548
RR1	9929.454	34.81914	15.83	0.0073	0.20347	0.6519	129.68	54.14377	0.582482
RR2	10123.35	35.93316	12.07	0.0178	5.4725	0.01932	70.61797	43.88292	0.378587
SS	10255.43	44.39034	4.647	0.164	0.41811	0.5179	69.06307	59.31634	0.141128
UUVV	10391.78	42.63297	0.417	0.536	0.91338	0.3392	33.77976	43.59357	-0.29052

3.3. Morphological Sources of Grain-Size Variability

Due to the long-tailed distribution of active channel widths (Figure 23), the logarithm of channel widths is used to evaluate the following hypothesis:

H4: Grain-sizes are negatively correlated with active channel width.

Grain-size varies significantly (decreases) with channel width based on an OLS linear regression, which produced an F-statistic of 77.97, a p-value less than $2.2e-16$, and an $r^2=0.1441$. There is significant variability in median grain-size within a given channel width, and particularly for narrow reaches (Figure 24). Visualizing the downbar position of each sample reveals that bar-scale location is a source of variability in the grain-size response to channel width (Figure 24). An additional OLS regression between median grain-size and active channel width for samples located at bar heads produced an F-statistic of 87.49, a p-value less than $2.2e-16$, and an $r^2=0.3606$. Active channel width may play a leading role in driving the downstream grain-size autocorrelation (Figure 20) since nearby observations are likely within similar channel conditions. Visualizing active channel width within the plot of grain-size vs. downstream distance shows the strong relationship between downstream patterns in grain-size and channel width (Figure 25).

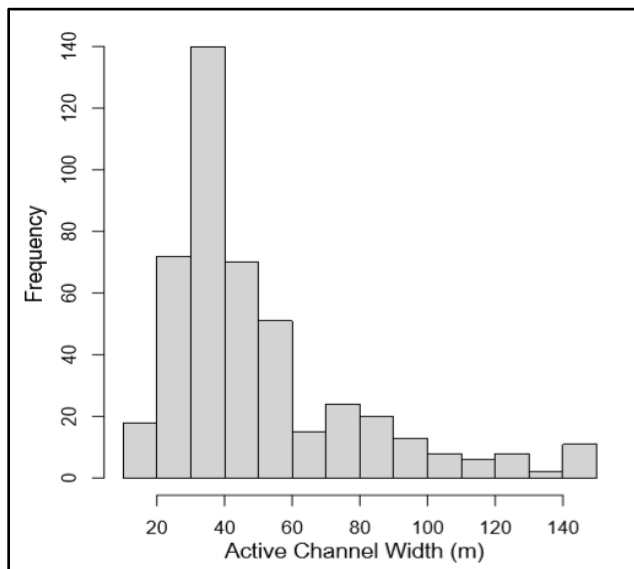


Figure 23: Histogram of the channel width at each grain-size sample location.

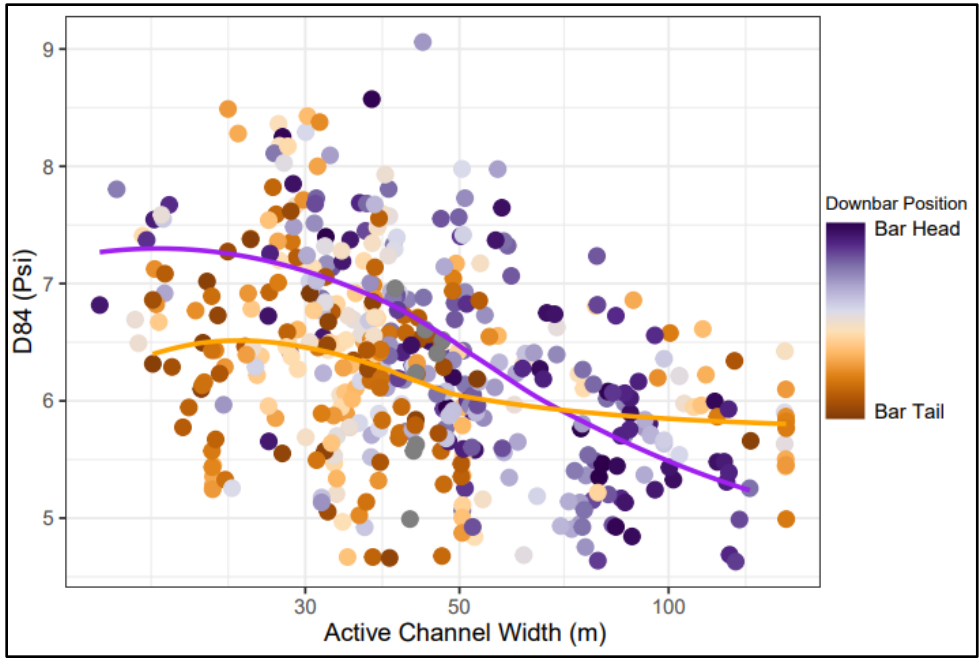


Figure 24: D84 vs. the active channel width for all samples within the study area. Downbar position is represented by sample colors. The purple line is fitted to samples located at the bar head and the orange line is fitted to bar tail samples.

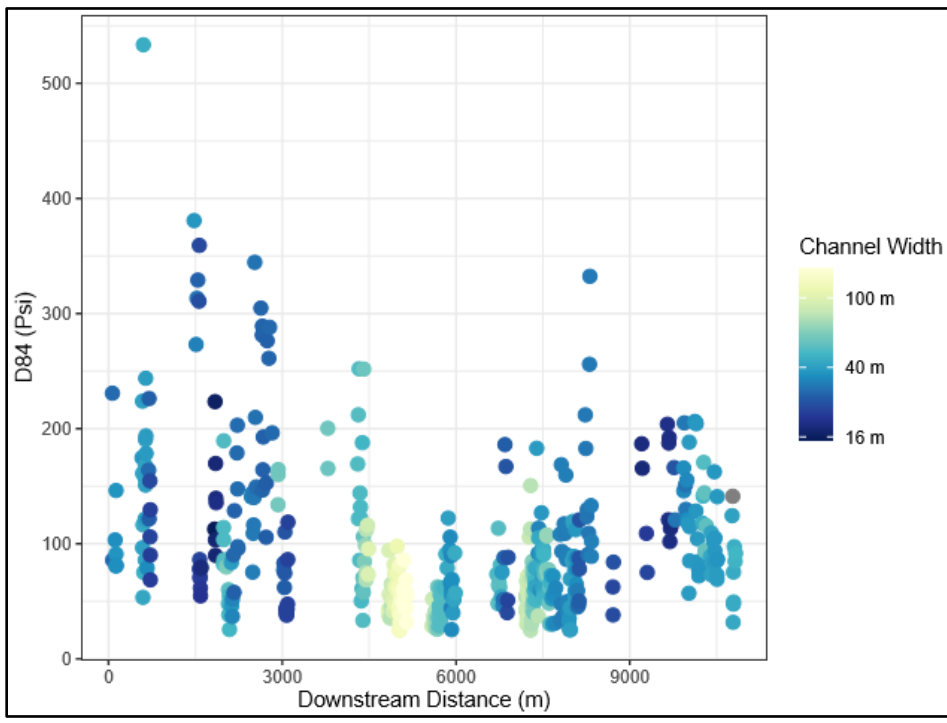


Figure 25: A multivariate plot showing D84 response to downstream position and channel width showing the importance of local channel morphology in driving downstream grain-size patterns.

4. Discussion

The results from Section 3 describe associations among grain-size, geomorphic attributes, and geographic position within the study area. The aim of this discussion is to leverage these associations to examine the sources of sediment grain-size variability in the Upper Sandy River and situate the results within the context of conceptual models of local versus upstream influences on sediment sorting. I focus on downstream grain-size patterns, the importance of active channel width, and bar-scale variability to discuss the implications of multiscale grain-size mapping in addressing the fundamental relationship between local grain-sizes and systematic patterns.

4.1. Surveying Limitations and Advantages

Characterizing the influence of the sampling strategy on the results is a prerequisite for the following interpretations regarding fluvial form and process. Comparisons between grain-size distributions measured through standard techniques such as the Wolman pebble count (Wolman, 1954) and an individual sample in this study are not appropriate due to the small areal extent for each sample survey. The sampling strategy was appropriate for this study given the explicit goal of comparing the spatial grain-size patterns at multiple scales within the study area. In order to produce a grain-size distribution that is comparable to other studies or other rivers, nearby samples would need to be aggregated to increase the sampling area following guidelines for areal sediment size surveying (Bunte and Abt, 2001). While this limits comparisons from individual samples in this dataset to grain-size distributions calculated elsewhere, future research could compare distributions calculated by aggregating patch-scale photosieved samples with traditional techniques.

The small sampling area likely contributes to the significant scatter shown within the results (e.g. Figures 22 and 25) since the grain-size distribution is calculated from relatively few grains positioned within a smaller spatial extent compared to traditional techniques. The scatter turns out to be one of the most interesting results of this study as it provides a distinct description of sediment within riverscapes when compared to standard grain-size measurement techniques. The impression of standard grain-size

distributions is that the percentiles of interest, such as median *b*-axis length, are characteristic of the grain-sizes throughout the sampling area. These results show that for the Upper Sandy this assumption is better suited to wider reaches with well sorted sediment (e.g. 4500-7500 m downstream in Figure 25), while the majority of the study site shows significant spread in the data within small areas such as an individual gravel bar (e.g. Figure 22).

4.2. Downstream Grain-Size Variability

The relationship between downstream position and fluvial physical features such as grain-size contextualizes observations at particular locations within larger extents. The River Continuum Concept (RCC) and Process Domains Concept (PDC) are two competing theoretical frameworks for defining the relationships among scales of geomorphic information. They share the approach of explaining local forms as a product of larger scale processes. Below, I discuss the implications of my results for H1 and H2 for the application of the RCC and PDC to understanding the Upper Sandy River.

The RCC is a multi-scalar hypothesis that describes a downstream continuous gradient of a river system's physical features (Vannote, 1980). The RCC is organized by dynamic equilibrium and sees rivers as adjusting towards a mean state, with deviations being caused by external factors such as geologic controls or disturbances. This focus on continuous downstream variations in channel morphology is based on downstream hydraulic geometry (DHG) (Leopold and Maddock, 1953). Downstream fining is a well-observed systematic pattern of sediment sorting at the channel length scale that reflects the application of the downstream continuum conception of fluvial systems to the grain-size variable. From this perspective, grain-size at a particular location is explained based on its position within a downstream fining sequence. Selective entrainment and deposition as well as abrasion are the physical processes behind downstream fining. Researchers have acknowledged that local processes may 'disrupt' these longitudinal patterns. Grain-size specific efforts to reconcile the influence of local conditions with systematic downstream fining led to amendments to downstream sediment sorting such as the Sediment Links Concept (Rice, 1998; Rice, 1999), which incorporates the effect of

lateral sediment sources into downstream grain-size patterns. Zettler-Mann and Fonstad (2020) used similar but more extensive drone-based grain-size remote sensing to evaluate the Sediment Links Concept on the Rogue River; however, the extent of the current study's multiscale grain-size map is too small to reveal a downstream fining sequence and the effect of lateral sediment sources such as hillslopes and tributaries. Instead, the resolution of the dataset lends itself to evaluating the sources of downstream variations in grain-sizes within the study area without a specific focus on fining sequences.

The longitudinal plot of grain-sizes in Figure 19 shows a distinct 3 km zone from 4500 m to 7500 m in which grain-sizes are smaller than those observed upstream and downstream. Figure 25 shows that this departure from the downstream trend is associated with a significantly wider active channel. While the sediment links concept seeks an explanation for disruptions to downstream fining where lateral sediment inputs produce a sudden increase in grain-sizes, these results suggest that systematic downstream trends are also disrupted due to decreased flow competency in wide reaches.

The PDC is an alternative approach that considers river forms within heterogeneous spatial zonations that are defined by a suite of geomorphic processes (Montgomery, 1999). In considering scale, Montgomery argues that regional characteristics including climate, geology, vegetation, and topography influence the process domain, which in turn determines the disturbance regime impacting the river corridor. From this vantage point, the physical features of the river system at a particular point have a range of variability that emerges from the disturbance regime – a stark contrast from the RCC's vision of continuous downstream changes in river morphology that are periodically 'disrupted' by local conditions.

This study's multiscale grain-size mapping results have important implications for Montgomery's proposed method for drawing process domain boundaries. The method suggests a hierarchical approach in which larger scale processes associated with tectonics and lithotopographic units allow the identification of discrete regions associated with geomorphic disturbance regimes (i.e. process domains). The spatially extensive observations of geomorphic variables such as grain-size may enable researchers to forego

the top-down hierarchical approach by defining process domain boundaries using geomorphic signals. Visual inspection of Figure 25 suggests a distinct process domain from 4500 m to 7500 m within the study area defined by decreased grain-sizes and increased active flow width. Continued advancements to riverscape mapping can enable bottom-up data driven analyses that use signal to noise ratios among hydrogeomorphic variables to reveal the spatially variable effect of large-scale process such as lithology.

The results of this study do not suggest that either the RCC or PDC is a superior conceptual model for the upper Sandy river. Instead, the aim is to communicate how multiscale fluvial mapping can enhance our understanding of river environments within both of these theoretical frameworks. A future application of multiscale mapping is to support the application of complexity science to river environments. Both RCC and PDC describe fluvial forms at particular locations within the context of the constraints of larger scale patterns and processes such as downstream fining or lithology. Complexity science takes a different approach by seeking explanations of how simple and fundamental processes at much smaller scales combine and produce systematic patterns and behavior (Malanson, 1999). Much of complexity science focuses on computer simulations, however its relevance to real world places will depend upon empirical observations at the scales of fundamental processes and the emerging systematic patterns.

4.3. Bar Scale Variability

Variations in local flow patterns around coarse sediment grain clusters (Brayshaw et al., 1883) and gravel bars (Ashworth et al., 1996) lead to bar scale bed material sorting during transport. Sediment sorting at this scale may play an important role in producing downstream fining if bar heads trap coarse material and reduce its availability to downstream reaches (Rice and Church, 2010). Despite the recognition that within-bar grain-size variability may have implications for downstream fining, bed load transport, and channel hydraulics, there have been relatively few examinations of bar scale grain-size sorting. Rice and Church (2010) examined grain-size variability within and among gravel bars on the Fraser River 50 km gravel reach. They found that individual bars contained on average 25% and up to 68% of the surface median grain-size range of the

entire study are. Figure 22 shows boxplots of the median grain-size distribution for individual bars within the Upper Sandy study site. The average range of patch-scale D_{50} within these bars was 34% of the study site with a single bar hosting 91% of the range of the study area. This increase relative to the Fraser gravel reach is expected given the smaller study site on the Upper Sandy. Both studies demonstrate the limitations of downstream fining models for understanding grain-sizes at spatial extents less than this 12 km study area given the impressive variability contained within bars.

Rice and Church also examined sorting based on longitudinal position on gravel bars. They found a 34% average head to tail decrease in median surface grain-size on their gravel bars, however this bar scale fining pattern decreased in the downstream distance due to a reduction in the size of the coarsest available grains. My bar scale sorting results in Table 3 suggest that longitudinal sorting is inconsistent – 14 of the 33 bars exhibited coarser bar tails than bar heads compared with 2 of 8 bars coarsening on the Fraser River. This variability in longitudinal bar scale sorting among gravel bars is a limitation to Rice and Church's proposed model for estimating local grain-sizes based on an expression for downstream fining to predict bar head grain-sizes combined with the average down-bar fining rate to predict the local median grain-size.

4.4. Grain-size association with active channel width

The inverse scaling relationship between active channel width and median b -axis length (Figure 24) emerged as the most important source of grain-size variability within our study area, which was likely too small for downstream fining to exert a significant control over grain-size. The cause of this relationship remains an outstanding question, but two hypotheses emerge from the results. The first potential explanation is that spatial differences in the grain-size of external sediment sources such as riverbanks enabled channel widening to occur in specific locations. The second hypothesis is that channel widening occurred in particular locations because of differences in lateral channel constraints, which produced differences in flow hydraulics that drove sediment sorting. Future research on the size of subsurface sediment within the widest reaches and the upper Sandy floodplain, or studies investigating the cause of future channel development

and widening would be necessary to definitively decide among these hypotheses.

The grain-size patterns within gravel bars and their relationship to channel width does provide insights into the role of flow hydraulics in sorting surface sediment. The active channel width variable is related to flow competence, which is the maximum transportable sediment grain-size through the channel at a given discharge (Charlton, 2007). Wider channels generally have a lower hydraulic radius resulting in decreased hydraulic efficiency, bed shear stress, and flow competence. This physical interaction among channel form and sediment movement likely encourages the decrease in grain-sizes associated with increased channel width throughout the study area. Channel width influences the median and variance of grain-sizes among patches. Specifically, narrow channels host the full range of grain-sizes observed in the study area while the coarsest patches do not occur in wide reaches (Figure 23). Given this result, what can explain the occurrence of coarse, medium, and fine patches within narrow channels?

Bar-scale position is an important source of grain-size variability within narrow channels. Figure 24 shows that the coarsest patches in the river appear at bar heads in narrow channels and that bar head grain-sizes decrease with increased channel width, while bar tail grain-sizes are less responsive to variations in width. At first glance, this result appears to contradict the boxplot comparing the distribution of median grain-sizes at bar heads and bar tails showing a longer median *b*-axis length at bar tails (Figure 21c). These observations can be reconciled by considering the larger spread in the grain-size distribution at bar heads, which is attributable to the coarser maximum patch-scale grain-size from samples located in narrow channels. The insignificant difference in median grain-size between bar heads and tails is likely due to the fact that bar tail grain-size is relatively unaffected by channel width leading to observed head to tail coarsening in wide channels (Table 6).

The differential response to active channel width among bar heads and tails suggests that flow competence calculations from channel cross-section dimensions are more suitable to understanding surface grain-sizes at bar heads, while bar tails are more consistent across morphological conditions. One hypothesis is that bar tail grain-size

distributions are reflective of secondary flow and local scale hydraulics from eddies, while bar heads are related to primary flow parallel to the channel centerline that is more subject to change with differences in channel width. Future research should investigate the agreement between conceptual models of bar development and sediment mobility with the observed pattern showing that the systematic relationship among channel width and grain-size is modulated by bar scale position.

5. Conclusions

This study argues that multiscale observations of fluvial physical characteristics may reveal systematic patterns that enable more detailed analyses of our physical explanations for fluvial process as well as our conceptual models relating local conditions with downstream patterns. I mapped the distribution of coarse sediment within 33 gravel bars along the upper Sandy River and analyzed the grain-size variability at the river segment and bar scales in related to active channel width. The results showed that grain-size was inversely correlated with channel width, but that this relationship was only significant for patches located at bar heads. Additionally, the results showed that local variability in some cases was nearly equivalent to the grain-size variability observed within the 12 km reach. This finding indicates that the application of downstream fining models may have limited application on the upper Sandy River at spatial extents smaller than approximately 1 km.

CHAPTER IV

CONCLUSION

Chapter 2 of this thesis addresses a methodological barrier to leveraging grain-size remote sensing techniques by presenting a methodological framework for image-based grain-size mapping. The framework describes the principal components photosieving. I outline the key decisions within the chain of grain-size map production and their implications for their resulting dataset. Given a set of research objectives for the upper Sandy River, I design a grain-size mapping protocol to efficiently survey grain-size variability within gravel bars and across a 12 km river segment.

Chapter 3 argues that multiscale observations of fluvial physical characteristics may reveal systematic patterns that enable more detailed analyses of our physical explanations for fluvial process as well as our conceptual models relating local conditions with larger scale downstream patterns. I map the distribution of coarse sediment within 33 gravel bars along the Upper Sandy River and analyze the grain-size variability at the river segment and bar scales in relation to active channel width. The results show that grain-size is inversely correlated with channel width, but that this relationship is only significant for patches located at bar heads. Additionally, the results illustrate that bar scale variability in some cases is nearly equivalent to the grain-size variability observed within the 12 km reach. This finding indicates that the application of downstream fining models may have limited application on the Upper Sandy River at scales finer than a few kilometers.

The limitations of this research include its focus solely on surface sediment. Image-based techniques are not capable of sampling subsurface sediment, which means traditional surveys will continue to be important for producing grain-size datasets. This surveying strategy also does not lead to continuous data of exposed gravel, which is a fundamental component of riverscape mapping. Future research will likely sacrifice the increased resolution of individual images to utilize the continuous coverage provided by orthomosaics as photosieving algorithms such as SediNet increase in accuracy and precision. An interesting opportunity would be to combine photosieving with land cover

classification, vegetation mapping, and topographic surveys to increase our understanding of various components of river morphology. A major limitation of this study is that it excludes in-channel geomorphic measurements and hydraulic information.

The advantages of this approach are its efficiency, accessibility, high resolution data, and relatively large spatial extent. The methodological approach enabled observations of the deviations from the systematic relationship between channel width and sediment grain-size based on downbar position, which also warrants further investigation to determine whether local sediment supply or hydraulics offer a more suitable explanation. Lastly, the upper Sandy River is dynamic through space and time. More surveys through time would enable a better understanding of channel development as future high flow events reshape the topography and texture of the river system.

REFERENCES CITED

CHAPTER I

- Carbonneau, P., Fonstad, M. A., Marcus, W. A., & Dugdale, S. J. (2012). Making riverscapes real. *Geomorphology*, 137(1), 74-86.
- Church, M., & Ferguson, R. I. (2015). Morphodynamics: Rivers beyond steady state. *Water Resources Research*, 51(4), 1883-1897.
- Dade, W. B. (2000). Grain size, sediment transport and alluvial channel pattern. *Geomorphology*, 35(1-2), 119-126.
- Fonstad, M. A., & Marcus, W. A. (2010). High resolution, basin extent observations and implications for understanding river form and process. *Earth Surface Processes and Landforms*, 35(6), 680-698.
- Handelman, C., Wise, S., Abbe, T., Reinhart, M.A., Higgins, S., & French, D. (2014) Restorative Flood Response Community Handbook. *Sandy River Watershed Council*.
- Kondolf, G. M., Sale, M. J., & Wolman, M. G. (1993). Modification of fluvial gravel size by spawning salmonids. *Water Resources Research*, 29(7), 2265-2274.
- Montgomery, D. R. (1999). Process domains and the river continuum. *Journal of the American Water Resources Association*, 35(2), 397-410.
- Paola, C., & Seal, R. (1995). Grain size patchiness as a cause of selective deposition and downstream fining. *Water Resources Research*, 31(5), 1395-1407.
- Powell, D. M. (1998). Patterns and processes of sediment sorting in gravel-bed rivers. *Progress in Physical Geography*, 22(1), 1-32.
- Van De Wiel, M. J., Coulthard, T. J., Macklin, M. G., & Lewin, J. (2007). Embedding reach-scale fluvial dynamics within the CAESAR cellular automaton landscape evolution model. *Geomorphology*, 90(3-4), 283-301.
- Vannote, R. L., Minshall, G. W., Cummins, K. W., Sedell, J. R., & Cushing, C. E. (1980). The river continuum concept. *Canadian Journal of Fisheries and Aquatic Sciences*, 37(1), 130-137.

CHAPTER II

- Adams, J. (1979). Gravel size analysis from photographs. *Journal of the Hydraulics Division*, 105(10), 1247-1255.
- Bathurst, J. C., Carling, P. A., Reid, I., Walling, D. E., & Webb, B. (1997). Sediment erosion, transport and deposition. *Applied Fluvial Geomorphology for River Engineering and Management*, Wiley, 95-135.

- Bunte, K., & Abt, S. R. (2001). Sampling surface and subsurface particle-size distributions in wadable gravel-and cobble-bed streams for analyses in sediment transport, hydraulics, and streambed monitoring. *US Department of Agriculture, Forest Service, Rocky Mountain Research Station*.
- Buscombe, D. (2008). Estimation of grain-size distributions and associated parameters from digital images of sediment. *Sedimentary Geology*, 210(1-2), 1-10.
- Buscombe, D. (2020). SediNet: A configurable deep learning model for mixed qualitative and quantitative optical granulometry. *Earth Surface Processes and Landforms*, 45(3), 638-651.
- Carbonneau, P. E., Lane, S. N., & Bergeron, N. E. (2004). Catchment-scale mapping of surface grain size in gravel bed rivers using airborne digital imagery. *Water Resources Research*, 40(7).
- Carbonneau, P. E., Bergeron, N., & Lane, S. N. (2005). Automated grain size measurements from airborne remote sensing for long profile measurements of fluvial grain sizes. *Water Resources Research*, 41(11).
- Carbonneau, P. E., & Dietrich, J. T. (2017). Cost-effective non-metric photogrammetry from consumer-grade sUAS: implications for direct georeferencing of structure from motion photogrammetry. *Earth Surface Processes and Landforms*, 42(3), 473-486.
- Carbonneau, P. E., Bizzi, S., & Marchetti, G. (2018). Robotic photosieving from low-cost multirotor sUAS: a proof-of-concept. *Earth Surface Processes and Landforms*, 43(5), 1160-1166.
- Cavalli, M., Tarolli, P., Marchi, L., & Dalla Fontana, G. (2008). The effectiveness of airborne LiDAR data in the recognition of channel-bed morphology. *Catena*, 73(3), 249-260.
- Chardon, V., Schmitt, L., Piégay, H., & Lague, D. (2020). Use of terrestrial photosieving and airborne topographic LiDAR to assess bed grain size in large rivers: a study on the Rhine River. *Earth Surface Processes and Landforms*, 45(10), 2314-2330.
- Church, M., & Ferguson, R. I. (2015). Morphodynamics: Rivers beyond steady state. *Water Resources Research*, 51(4), 1883-1897.
- Dade, W. B. (2000). Grain size, sediment transport and alluvial channel pattern. *Geomorphology*, 35(1-2), 119-126.
- Detert, M., & Weitbrecht, V. (2013). User guide to gravelometric image analysis by BASEGRAIN. *Advances in Science and Research*, 1789-1795.
- Dietrich, J.T. (2019). Py_streamNormalcoords. https://github.com/geojames/py_streamNormalcoords. (Accessed February 2021).

- East, A. E., Jenkins, K. J., Happe, P. J., Bountry, J. A., Beechie, T. J., Mastin, M. C., ... & Randle, T. J. (2017). Channel-planform evolution in four rivers of Olympic National Park, Washington, USA: the roles of physical drivers and trophic cascades. *Earth Surface Processes and Landforms*, 42(7), 1011-1032.
- Fonstad, M. A., & Marcus, W. A. (2010). High resolution, basin extent observations and implications for understanding river form and process. *Earth Surface Processes and Landforms*, 35(6), 680-698.
- Fonstad, M. A., Dietrich, J. T., Courville, B. C., Jensen, J. L., & Carbonneau, P. E. (2013). Topographic structure from motion: a new development in photogrammetric measurement. *Earth Surface Processes and Landforms*, 38(4), 421-430.
- Fonstad, M. A., & Zettler-Mann, A. (2020). The camera and the geomorphologist. *Geomorphology*, 366, 107181.
- Graham, D. J., Rice, S. P., & Reid, I. (2005). A transferable method for the automated grain sizing of river gravels. *Water Resources Research*, 41(7).
- Graham, D. J., Rollet, A. J., Piégay, H., & Rice, S. P. (2010). Maximizing the accuracy of image-based surface sediment sampling techniques. *Water Resources Research*, 46(2).
- Kondolf, G. M., Sale, M. J., & Wolman, M. G. (1993). Modification of fluvial gravel size by spawning salmonids. *Water Resources Research*, 29(7), 2265-2274.
- Lang, N., Irniger, A., Rozniak, A., Hunziker, R., Wegner, J. D., & Schindler, K. (2020). GRAINet: Mapping grain size distributions in river beds from UAV images with convolutional neural networks. *Hydrology and Earth System Sciences Discussions*, 1-38.
- Lee, A. J., & Ferguson, R. I. (2002). Velocity and flow resistance in step-pool streams. *Geomorphology*, 46(1-2), 59-71.
- Legleiter, C. J., & Kyriakidis, P. C. (2006). Forward and inverse transformations between Cartesian and channel-fitted coordinate systems for meandering rivers. *Mathematical Geology*, 38(8), 927-958.
- Marcus, W. A., & Fonstad, M. A. (2010). Remote sensing of rivers: the emergence of a subdiscipline in the river sciences. *Earth Surface Processes and Landforms*, 35(15), 1867-1872.
- Nelson, P. A., Bellugi, D., & Dietrich, W. E. (2014). Delineation of river bed-surface patches by clustering high-resolution spatial grain size data. *Geomorphology*, 205, 102-119.
- O'Connor, J. E., Jones, M. A., & Haluska, T. L. (2003). Flood plain and channel dynamics of the Quinault and Queets Rivers, Washington, USA. *Geomorphology*, 51(1-3), 31-59.

- Paola, C., & Seal, R. (1995). Grain size patchiness as a cause of selective deposition and downstream fining. *Water Resources Research*, 31(5), 1395-1407.
- Piégay, H., Arnaud, F., Belletti, B., Bertrand, M., Bizzi, S., Carbonneau, P., ... & Slater, L. (2020). Remotely sensed rivers in the Anthropocene: State of the art and prospects. *Earth Surface Processes and Landforms*, 45(1), 157-188.
- Powell, D. M. (1998). Patterns and processes of sediment sorting in gravel-bed rivers. *Progress in Physical Geography*, 22(1), 1-32.
- Purinton, B., & Bookhagen, B. (2019). Introducing PebbleCounts: a grain-sizing tool for photo surveys of dynamic gravel-bed rivers. *Earth Surface Dynamics*, 7(3), 859-877.
- Reid, I., Powell, D. M., & Laronne, J. B. (1996). Prediction of bed-load transport by desert flash floods. *Journal of Hydraulic Engineering*, 122(3), 170-173.
- Rengers, F., & Wohl, E. (2007). Trends of grain sizes on gravel bars in the Rio Chagres, Panama. *Geomorphology*, 83(3-4), 282-293.
- Rice, S., & Church, M. (1998). Grain size along two gravel-bed rivers: statistical variation, spatial pattern and sedimentary links. *Earth Surface Processes and Landforms*, 23(4), 345-363.
- Rice, S. P., & Church, M. (2010). Grain-size sorting within river bars in relation to downstream fining along a wandering channel. *Sedimentology*, 57(1), 232-251.
- Rice, S. (1998). Which tributaries disrupt downstream fining along gravel-bed rivers?. *Geomorphology*, 22(1), 39-56.
- Robert, A. (1990). Boundary roughness in coarse-grained channels. *Progress in Physical Geography*, 14(1), 42-70.
- Schumm, S. A., & Lichty, R. W. (1965). Time, space, and causality in geomorphology. *American Journal of Science*, 263(2), 110-119.
- Seal, R., & Paola, C. (1995). Observations of downstream fining on the North Fork Toutle River near Mount St. Helens, Washington. *Water Resources Research*, 31(5), 1409-1419.
- Smith, J. D., & McLean, S. R. (1984). A model for flow in meandering streams. *Water Resources Research*, 20(9), 1301-1315.
- Van De Wiel, M. J., Coulthard, T. J., Macklin, M. G., & Lewin, J. (2007). Embedding reach-scale fluvial dynamics within the CAESAR cellular automaton landscape evolution model. *Geomorphology*, 90(3-4), 283-301.
- Wolman, M. G. (1954). A method of sampling coarse river-bed material. *EOS, Transactions American Geophysical Union*, 35(6), 951-956.
- Zettler-Mann, A., & Fonstad, M. (2020). Riverscape mapping and hyperscale analysis of the sediment links concept. *Geomorphology*, 350, 106920.

CHAPTER III

- Ashworth, P. J. (1996). Mid-channel bar growth and its relationship to local flow strength and direction. *Earth Surface Processes and Landforms*, 21(2), 103-123.
- Brayshaw, Andrew C., Lynne E. Frostick, and I. A. N. Reid. (1983). The hydrodynamics of particle clusters and sediment entrapment in coarse alluvial channels. *Sedimentology* 30(1), 137-143.
- Cameron, K. A., & Pringle, P. (1986). Post-glacial lahars of the Sandy River Basin, Mount Hood, Oregon. *Northwest Science*, 60(4), 225-237.
- Cavalli, M., Tarolli, P., Marchi, L., & Dalla Fontana, G. (2008). The effectiveness of airborne LiDAR data in the recognition of channel-bed morphology. *Catena*, 73(3), 249-260.
- Carbonneau, P., Fonstad, M. A., Marcus, W. A., & Dugdale, S. J. (2012). Making riverscapes real. *Geomorphology*, 137(1), 74-86.
- East, A. E., Jenkins, K. J., Happe, P. J., Bountry, J. A., Beechie, T. J., Mastin, M. C., ... & Randle, T. J. (2017). Channel-planform evolution in four rivers of Olympic National Park, Washington, USA: the roles of physical drivers and trophic cascades. *Earth Surface Processes and Landforms*, 42(7), 1011-1032.
- Dietrich, J. T. (2016). Riverscape mapping with helicopter-based Structure-from-Motion photogrammetry. *Geomorphology*, 252, 144-157.
- Dietrich, J.T. (2019). Py_streamNormalcoords.
https://github.com/geojames/py_streamNormalcoords. (Accessed February 2021).
- Fonstad, M. A., & Marcus, W. A. (2010). High resolution, basin extent observations and implications for understanding river form and process. *Earth Surface Processes and Landforms*, 35(6), 680-698.
- Fonstad, M. A., Dietrich, J. T., Courville, B. C., Jensen, J. L., & Carbonneau, P. E. (2013). Topographic structure from motion: a new development in photogrammetric measurement. *Earth Surface Processes and Landforms*, 38(4), 421-430.
- Fonstad, M. A., & Zettler-Mann, A. (2020). The camera and the geomorphologist. *Geomorphology*, 366, 107181.
- Handelman, C., Wise, S., Abbe, T., Reinhart, M.A., Higgins, S., & French, D. (2014) Restorative Flood Response Community Handbook. *Sandy River Watershed Council*.
- Legleiter, C. J., & Kyriakidis, P. C. (2006). Forward and inverse transformations between Cartesian and channel-fitted coordinate systems for meandering rivers. *Mathematical Geology*, 38(8), 927-958.
- Leopold, L. B., & Maddock, T. (1953). The hydraulic geometry of stream channels and some physiographic implications. (Vol. 252). *US Government Printing Office*.

- Malanson, G. P. (1999). Considering complexity. *Annals of the American Association of Geographers*, 89(4), 746-753.
- Montgomery, D. R. (1999). Process domains and the river continuum. *Journal of the American Water Resources Association*, 35(2), 397-410.
- Parker, G., & Klingeman, P. C. (1982). On why gravel bed streams are paved. *Water Resources Research*, 18(5), 1409-1423.
- Parker, G., Dhamotharan, S., & Stefan, H. (1982). Model experiments on mobile, paved gravel bed streams. *Water Resources Research*, 18(5), 1395-1408.
- Parker, G. (1991). Selective sorting and abrasion of river gravel. II: Applications. *Journal of Hydraulic Engineering*, 117(2), 150-171.
- Paola, C., & Seal, R. (1995). Grain size patchiness as a cause of selective deposition and downstream fining. *Water Resources Research*, 31(5), 1395-1407.
- Piégay, H., Arnaud, F., Belletti, B., Bertrand, M., Bizzi, S., Carbonneau, P., & Slater, L. (2020). Remotely sensed rivers in the Anthropocene: State of the art and prospects. *Earth Surface Processes and Landforms*, 45(1), 157-188.
- Powell, D. M. (1998). Patterns and processes of sediment sorting in gravel-bed rivers. *Progress in Physical Geography*, 22(1), 1-32.
- Purinton, B., & Bookhagen, B. (2019). Introducing PebbleCounts: a grain-sizing tool for photo surveys of dynamic gravel-bed rivers. *Earth Surface Dynamics*, 7(3), 859-877.
- Rice, S. (1998). Which tributaries disrupt downstream fining along gravel-bed rivers?. *Geomorphology*, 22(1), 39-56.
- Rice, S. (1999). The nature and controls on downstream fining within sedimentary links. *Journal of Sedimentary Research*, 69(1), 32-39.
- Richards, K., & Clifford, N. (1991). Fluvial geomorphology: structured beds in gravelly rivers. *Progress in Physical Geography*, 15(4), 407-422.
- Seal, R., & Paola, C. (1995). Observations of downstream fining on the North Fork Toutle River near Mount St. Helens, Washington. *Water Resources Research*, 31(5), 1409-1419.
- Vannote, R. L., Minshall, G. W., Cummins, K. W., Sedell, J. R., & Cushing, C. E. (1980). The river continuum concept. *Canadian Journal of Fisheries and Aquatic Sciences*, 37(1), 130-137.
- Wolman, M. G. (1954). A method of sampling coarse river-bed material. *EOS, Transactions American Geophysical Union*, 35(6), 951-956.
- Zettler-Mann, A., & Fonstad, M. (2020). Riverscape mapping and hyperscale analysis of the sediment links concept. *Geomorphology*, 350, 106920.